Liu, J., Nowaczyk, N., Jiang, X., Zhong, Y., Wirth, R., Liu, Q., Arz, H. W. (2022): Holocene Paleosecular Variations Recorded by Relict Magnetic Minerals in the Anoxic Black Sea Sediments. - Journal of Geophysical Research: Solid Earth, 127, 5, e2022JB024179.

https://doi.org/10.1029/2022JB024179

JGR Solid Earth

RESEARCH ARTICLE
10.1029/2022JB024179

Holocene Paleosecular Variations Recorded by Relict Magnetic Minerals in the Anoxic Black Sea Sediments

Jiabo Liu[1,2], Norbert R. Nowaczyk[3], Xiaodong Jiang[1], Yi Zhong[1], Richard Wirth[4], Qingsong Liu[1,5,6], and Helge W. Arz[7]

[1]Centre for Marine Magnetism (CM[2]), Department of Ocean Science and Engineering, Southern University of Science and Technology, Shenzhen, China, [2]Key Laboratory of Marine Geology and Metallogeny, MNR, Qingdao, China, [3]Helmholtz Centre Potsdam, GFZ German Research Centre for Geosciences, Section 4.3, Potsdam, Germany, [4]Helmholtz Centre Potsdam, GFZ German Research Centre for Geosciences, Section 3.5, Potsdam, Germany, [5]Shanghai Sheshan National Geophysical Observatory, Shanghai, China, [6]Southern Marine Science and Engineering Guangdong Laboratory, Guangzhou, China, [7]Leibniz Institute for Baltic Sea Research Warnemünde, Marine Geology, Rostock, Germany

Abstract Continuous paleosecular variations reconstructed from sedimentary archives have remarkably deepened our insights into the dynamics of the Earth's magnetic field as well as the chronological purpose. Nevertheless, to construct reliable sedimentary paleomagnetic records in diagenetic reducing sediments is challenging generally due to the pervasive magnetic mineral diagenesis. The relict magnetic minerals are residuals after diagenesis and probably able to record a depositional remanent magnetization, thus it is worthy to explore their paleomagnetic potentials. For this study, two Black Sea sediment cores covering the past 8 ka were subjected to mineralogical and paleo- and rock magnetic analyses. Paramagnetic pyrite framboids are pervasive in the studied sediments deposited under anoxic bottom water conditions in the Black Sea. In addition, relict magnetic minerals of ferrous hemoilmenite, Fe-Mn and Fe-Cr spinels, and magnetite inclusions are also present in the studied cores. Compared to the previous published paleomagnetic results from the same cores over the last glacial period (20–30 ka) which are dominated by detrital (titano-)magnetite particles, the studied relict magnetic mineral samples exhibit a similar behavior in recording the depositional remanent magnetization. Furthermore, the obtained paleosecular variations spanning the past 8 ka reproduce the high intensity patterns observed in the regional archeomagnetic and volcanic datasets. Thus, the successful reconstruction of paleomagnetic secular variations from the anoxic Black Sea sediments greatly extend the application of paleomagnetism in sediments deposited in water with a reducing sub-surface environments from where paleomagnetic data are generally sparse.

Plain Language Summary The Earth's magnetic field can be recorded by magnetic minerals during their deposition within a water column, and are later preserved in sediments. The geomagnetic field signal may be biased if the magnetic minerals are subsequently altered because of changes in bottom water redox conditions. However, relict magnetic minerals are resistant to ambient environmental changes and thus have great potentials to record reliable paleomagnetic signals. To attest this novel idea, we systematically investigated sediments form the Black Sea under strong anoxic bottom water conditions. Our results demonstrate that the relict magnetic minerals survived in the Black Sea sediments covering the past eight thousand years. By comparison with detrital (titano-)magnetite samples, we found that relict magnetic mineral samples have similar behavior in recording the geomagnetic field. Moreover, the geomagnetic field variations reconstructed from the Black Sea sediments are comparable with other validated regional datasets for the past eight thousand years. Therefore, our new study significantly extends the application of paleomagnetic methods in a wider range of sedimentary redox conditions.

Key Points:

- Relict minerals of hemoilmenite, Fe-Mn and Fe-Cr spinels, and magnetic inclusions are magnetic carriers in studied Black Sea sediments
- The ability in recording the DRM by relict magnetic minerals are comparable with detrital (titano-) magnetite
- The obtained paleosecular variations resemble reginal field patterns observed in archeomagnetic and volcanic datasets for the past 8 ka

Supporting Information:

Supporting Information may be found in the online version of this article.

Correspondence to:

J. Liu,
liujiabo7@gmail.com

Citation:

Liu, J., Nowaczyk, N. R., Jiang, X., Zhong, Y., Wirth, R., Liu, Q., & Arz, H. W. (2022). Holocene paleosecular variations recorded by relict magnetic minerals in the anoxic Black Sea sediments. *Journal of Geophysical Research: Solid Earth*, *127*, e2022JB024179. https://doi.org/10.1029/2022JB024179

Received 7 FEB 2022
Accepted 2 MAY 2022

1. Introduction

The Earth's magnetic field, comprising relative paleointensity (RPI) and directions, can be recorded by magnetic minerals during their deposition in the water column via the depositional remanent magnetization (DRM) and the post DRM (PDRM) mechanisms (Tauxe et al., 2006). Given the advantage of continuity, paleomagnetic results derived from sedimentary archives have been broadly used in deciphering the evolution of Earth's magnetic field and determining chronology (e.g., Channell et al., 2020; Lund et al., 2006; Nowaczyk et al., 2012; Panovska et al., 2019; Stoner et al., 2002; Valet & Fournier, 2016). However, recovering reliable paleomagnetic data

from sediments is challenging (e.g., Bilardello et al., 2013; Gilder et al., 2019; Katari & Tauxe, 2000; Selkin et al., 2000; Tauxe, 1993), one of the major issues is the magnetic mineral diageneses associated with changing ambient environments (Ebert et al., 2021; Roberts, 2015; Wiers et al., 2019). Following the formation of secondary magnetic minerals in sediments, a chemical remanent magnetization (CRM) is formed, contemporaneously overlapping with and/or replacing the original DRM (e.g., Channell & Xuan, 2009; Dekkers & Rochette, 1992; Hus, 1990; Rowan et al., 2009; Snowball, 1997; Snowball & Thompson, 1990). Specifically, depositional environments during interglacial are featuring magnetic minerals diagenesis by reasons of abundant organic input and/or weak ventilations (Jianxing Liu et al., 2014; Larrasoaña et al., 2003; Roberts, 2015). Thus, paleomagnetic results derived from interglacial sediments are generally problematic (e.g., Just et al., 2019).

In reducing environments, detrital (titano-)magnetite undergoes dissolution and release Fe^{2+} which can react rapidly with HS^- from the water column to form iron sulfides (Canfield & Berner, 1987; Roberts, 2015). Instead, relict minerals of ilmenite, Fr-Cr and Fe-Mn spinels can resist against dissolution due to their low content of iron (Canfield et al., 1992). Accordingly, relict magnetic mineral assemblages, including the magnetic inclusions protected by silicates, are residuals of detrital magnetic minerals after diagenesis and widely found in reducing environments (e.g., Chang et al., 2016; Hounslow, 1996; Just et al., 2012; Nowaczyk, 2011; Wilson & Roberts, 1999). The paleomagnetic significances of magnetic inclusions have been broadly investigated in igneous rocks (e.g., Feinberg et al., 2005; Tarduno et al., 2006; Usui et al., 2015) and recently in sedimentary archives (Chang et al., 2021; Chen et al., 2017; Hong et al., 2019). It is found that magnetic inclusions are able to record the geomagnetic field, but have a lower efficiency in recording the DRM than other detrital magnetic minerals (Chang et al., 2021; Hong et al., 2019). Although ilmenite is paramagnetic at room temperature, ilmenite grains that contain submicron domains of a single domain (SD) ferrimagnetic hemoilmenite phase is likely responsible for the measured paleomagnetic signals (Lawson & Nord, 1984; Wilson & Roberts, 1999). In addition, Robinson et al. (2002) suggested that ilmenite can record magnetic signals by lamellar magnetism. Hounslow (1996) reported that ferrimagnetic Fe-Cr and Fe-Mn spinels are the dominant remanence carrying phases in the Lunde Formation, North Sea. And the Fe-Cr spinel is also a potential carrier of a natural remanent magnetization (NRM) and a source of magnetic anomalies in ultramafic complexes (Yu & Tikoff, 2020). From sediments which are dominated by ferrous ilmenites, (titano-)magnetite, Cr-Fe spinels, and impure magnetite, Scheidt et al. (2017) also reconstructed a reliable magnetic polarity stratigraphy. Hence, the relict magnetic minerals which can survive in reducing environments are promising to record the geomagnetic field in sediments where other detrital magnetic minerals were dissolved and no secondary magnetic minerals formed.

The highly variable paleosecular variations spanning the Holocene are characterized by a series of high and low intensity anomalies which were found in archeomagnetic and volcanic data (e.g., Ben-Yosef et al., 2009; Cai et al., 2021; Kovacheva et al., 2014; Shaar et al., 2016; Tarduno et al., 2015). At about 3 ka BP, the Levantine Iron Age Anomaly (LIAA) with high intensity and rapid secular variations was firstly reported from the Levant region (Ben-Yosef et al., 2009; Shaar et al., 2016) and later found around the Mediterranean region (Molina-Cardín et al., 2018; Osete et al., 2020; Rivero-montero, Gómez-Paccard, Kondopoulou, et al., 2021). An additional high field intensity at ∼1.2 ka BP with a double-oscillation feature was commonly observed in European archeomagnetic results (e.g., Genevey et al., 2016; Gómez-Paccard et al., 2012; Kovacheva et al., 2014), though the maxima do not occur simultaneously in Western and Eastern Europe (Rivero-Montero, Gómez-Paccard, Pavón-Carrasco, et al., 2021). During the past millennia, low paleointensity anomalies were found in southern Africa (∼650 years BP; Tarduno et al., 2015), and southern Asia (∼750 years BP; Cai et al., 2021). Presently, the geomagnetic field intensity is decreasing driven by the growing South Atlantic Anomaly. Aiming to decipher the origin and evolutions of these intensity fluctuations, as well as their relations with the Earth's core dynamics (Davies & Constable, 2017; Korte & Constable, 2018), it is essential to improve paleomagnetic data with increasing temporal and spatial coverages (Panovska et al., 2019). Specifically, sedimentary paleosecular variations (PSV) which are continuous and reach further back in time than archeomagnetic data can provide valuable information about the evolution of the Holocene geomagnetic field (Béguin et al., 2019).

Here, we present paleomagnetic results from two Black Sea sediment cores spanning the past 8 ka, coeval with the Holocene period. The Black Sea is the world's largest anoxic basin and is a semi-closed basin that was connected to the Marmara and Mediterranean Seas since about 9.5 ka (Badertscher et al., 2011; Bahr et al., 2008; Lamy et al., 2006; Soulet et al., 2011; Wegwerth et al., 2018). After the reconnection, the constant anoxic Black Sea bottom water favors diagenesis of a steady-state pattern (e.g., Berner, 1984), and pervasive pyrite framboids were

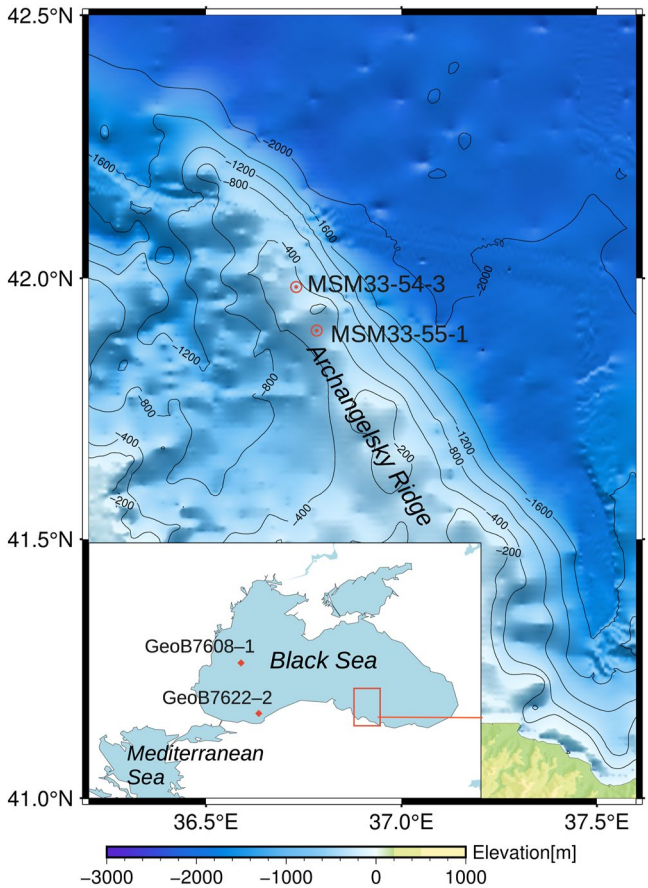

Figure 1. Bathymetric map of the SE Black Sea. Sediment cores MSM33-55-1 and MSM33-54-3 were taken along the center of the Archangelsky Ridge during RV *Maria S. Merian* expedition MSM33 in 2013. Sediment cores GeoB7608-1 and GeoB7622-2 were taken from the western Black Sea during RV *Meteor* expedition M51/4.

reported in the Black Sea sapropelic sediments since about 8.3 ka (Peckmann et al., 2001; Wilkin et al., 1996). With respect to the paramagnetic pyrite, the ferrimagnetic greigite which commonly cause biased paleomagnetic results (e.g., Rowan et al., 2009) have not been observed in previous studies in the Black Sea sapropels (e.g., Peckmann et al., 2001; Wilkin et al., 1997). In this study, detailed mineralogical and rock magnetic results demonstrate that the relict magnetic minerals are the magnetic carriers in the Holocene Black Sea sediments. In contrast, previous studies revealed that detrital (titano-)magnetite minerals are in dominance in the last glacial (14–70 ka) Black Sea sediments (Jiabo Liu et al., 2019; Nowaczyk et al., 2012, 2018). By comparing paleomagnetic results with data on the same cores from the last glacial period (20–30 ka), as well as with other regional paleomagnetic records, potential implications of the PSV derived from relict magnetic mineral samples from the Holocene Black Sea sediments are discussed.

2. Materials and Methods

2.1. Sediments

At the Archangelsky Ridge, Black Sea, a total of 18 sediment cores were taken by German RV *Meteor* in 2007 (leg M72/5) and RV *Maria S. Merian* in 2013 (leg MSM33). During the last glacial, the Black Sea was a giant freshwater lake, and the glacial sediments characterized by (titano-)magnetite minerals were used to reconstruct the PSV spanning from 14 to 70 ka (Jiabo Liu et al., 2020; Nowaczyk et al., 2013). After the Mediterranean Sea water ingression, finely laminated organic-rich sapropelic sediments and coccolith oozes were deposited in the Black Sea since about 8.3 ka (e.g., Bahr et al., 2005; Shumilovskikh et al., 2013). The studied Black Sea sapropels are characterized by variable carbonate (total inorganic carbon: 1.1%–9.8%) and organic matter (total organic carbon: 0.1%–12.2%) contents (Wegwerth et al., 2018). Framboids of paramagnetic pyrite were commonly formed as a result of the organo-clastic sulphate (SO_4^{2-}) reduction and the sulphate reduction coupled to anaerobic oxidation of methane (SO_4-AOM; e.g., Egger et al., 2016; Jørgensen et al., 2004; Neretin et al., 2004; Peckmann et al., 2001; Wilkin et al., 1996). According to the age models shown by Jiabo Liu et al. (2020), cores MSM33-55-1 and MSM33-54-3 (Figure 1) covering the Holocene period with relatively higher sedimentation rates (10.75 cm/kyr and 12.6 cm/kyr, respectively) than the other cores were subjected to detailed paleo- and rock magnetic investigations for this study. The whole paleo- and rock magnetic data from the cores MSM33-55-1 and MSM33-54-1 are presented in Jiabo Liu et al. (2019) and Nowaczyk et al. (2018), respectively. Since the two cores have identical rock magnetic properties for the Holocene interval, further rock magnetic and mineralogical analyses were performed on selected samples only from core MSM33-55-1.

2.2. Magnetic Extraction

Two magnetic extraction samples were prepared from depth 20.4 and 71.0 cm from core MSM33-55-1. Fresh sediments (~2 cm^3) taken from paleomagnetic sample boxes (6 cm^3) were dissolved into about 50 cm^3 of ethanol. The resulting slurry was dispersed and whirled for 5 min using ultrasound. The procedures of extracting magnetic minerals followed Nowaczyk (2011) with the probe of type B, a complete 2 cm diameter magnet placed inside a plastic probe submerged into the diluted sediment slurry with ultrasound action for 2 min. After turning off the ultrasound, the probe was moved gently in the slurry for about 1 min. Then the probe was taken out and placed into a small vial. After gently taking the magnet out, the magnetically attracted material at the outside of the probe is washed off using ethanol. By repeating the extracting procedures 5–10 times, magnetic materials are accumulating in the ethanol solution in the vial. For electron microscopic observations, 2–3 drops of the collected ethanol solution with magnetic material were dropped on the sample holders.

2.3. Scanning and Transmission Electron Microscope

Scanning electron microscope (SEM) imaging, together with energy dispersive X-ray spectroscopy (EDS) analysis, were performed on standard SEM stubs for bulk sediments (18 cm, 20.4 and 71.0 cm) and magnetic extractions (20.4 and 71.0 cm) from core MSM33-55-1. For SEM imaging, all samples of this study were sputtered with carbon (C). The electron backscatter mode was used for SEM observations. The SEM measurements for bulk sediments were performed using a Carl Zeiss SMT Ultra 55 Plus, generally with a voltage of 20 kV, an aperture of 120 μm, and a working distance of ∼12 mm. The measurements of bulk sediments were conducted at the Helmholtz Centre Potsdam, GFZ German Research Centre for Geosciences, Potsdam, Germany. With similar settings, magnetic extraction samples were analyzed using a Carl Zeiss Sigma 300 VP, equipped with a Bruker QUANTAX EDS at the department of Earth and Space Science, Southern University of Science and Technology (SUSTECH), Shenzhen, China.

The transmission electron microscope (TEM) foil was prepared from magnetic extractions from depth 20.4 cm from core MSM33-55-1 following Wirth (2004, 2009). The TEM observations were performed using a FEI Tecnai G2 F20 X-Twin TEM with a Schottky field emitter as an electron source. The TEM was equipped with a Fishione high-angle annular dark-field detector (HAADF), and an EDAX X-ray analyzer. High-resolution lattice fringe images were used to calculate the diffraction pattern (fast Fourier transform, FFT) of minerals. The observed d-spacings and angles between adjacent planes were compared with the d-spacings and angles calculated from literature data. The TEM analyses were conducted at the GFZ, Potsdam, Germany.

2.4. Dissolution Experiments

Bulk sediments from depth 20.4 and 71.0 cm from core MSM33-55-1 were freeze-dried for 24 hr at −50°C and vacuum conditions. Then the two samples (0.103 and 0.159 g) were ground to 200 mesh powder, and treated with 30 mL HCL solution (10 mol/L) for 24 hr in a 100 mL conical flask. The reactions were performed on a tabletop centrifuge with 150 revolutions per minute (rpm) at 35°C. After the reaction, samples were transported to a 50-mL tube for centrifugation at 4,500 rpm for 10 min. After removal of the supernatant fluid, the samples were washed with ultrapure water three times. More detailed procedures are described by Jiang et al. (2021). The obtained residuals and untreated samples were freeze-dried again and used for later rock magnetic measurements. For SEM observations, two magnetic extraction samples were prepared from the residuals following the magnetic extracting procedures described in Section 2.2.

2.5. Paleo- and Rock Magnetism

Discrete samples from cores MSM33-55-1 and MSM33-54-3 were taken by using rectangular plastic boxes (inner dimension 20 × 20 × 15 mm) with a volume of 6 cm^3. The low-frequency magnetic volume susceptibility κ_{LF} was determined by using an AGICO Multi-function Kappabridge MFK1-A, applying a field of 200 $Am.^{-1}$ and a frequency of 976 Hz. Temperature-dependent κ_{LF} measurements up to 700°C in argon atmosphere were also performed by using the MFK1-A in combination with a CS-3 unit.

The NRM and the anhysteretic remanent magnetization (ARM) were measured with a cryogenic 2G Enterprises 755 SRM long-core magnetometer. The NRM was alternating field (AF) demagnetized in steps of 0, 5, 10, 15, 20, 30, 40, 50, 65, 80, and 100 mT. Characteristic remanent magnetization (ChRM) directions were determined by using principal component analysis (PCA) following Kirschvink (1980). Directional maximum angular dispersions (MAD) of individual samples are converted to α_{95} uncertainties following Heslop and Roberts (2020). The ARM was imparted along the samples' z-axes with a static field of 0.05 mT and an AF field of 100 mT. AF demagnetization of the ARM was performed in steps of 0, 10, 20, 30, 40, 50, 65, and 80 mT. The slope of NRM versus ARM of common demagnetization steps along a straight line is defined as the relative paleointensity (RPI). A 2 G Enterprises 660 pulse magnetizer was used to impart an isothermal remanent magnetization (IRM), with the IRM acquired in a field of 1,500 mT defined as the saturation IRM (SIRM). The samples' IRMs were measured with a Molyneux spinner magnetometer. All paleo- and rock magnetic measurements for discrete samples were conducted at the GFZ, Potsdam, Germany.

Freeze-dried bulk sediments (18.0 cm, 20.4 cm, 71.0 cm and 80.2 cm), and the residuals (20.4 and 71.0 cm) after the dissolution experiments from core MSM33-55-1 were subjected to detailed rock magnetic measurements.

IRM acquisition curves were obtained by applying 61 logarithmically spaced field steps from 2 mT to 1 T. The IRM component analyses were calculated using the software "pyIRM", based on a Gaussian mixture model, available on https://github.com/botaoxiongyong/pyIRM. The protocol and calculation of irregular spaced first order reversal curve (irFORC) and transient hysteresis-free FORC (tfFORC) diagrams were performed following Zhao et al. (2015, 2017). All FORC diagrams were calculated with a smooth factor (SF) of 3 using the software "XFORC" (Zhao et al., 2015, 2017). The FORC, hysteresis curves and IRM acquisition curves were measured on a LakeShore vibrating sample magnetometer (VSM) 8600 at the SUSTECH, Shenzhen, China.

Low-temperature magnetic properties were measured using a Quantum Design Magnetic Property Measurement System (MPMS) at the Helmholtz-Zentrum Berlin (HZB), Germany. Magnetic extractions from sediments from 80.2 cm were cooled to 5 K in either zero field (ZFC) or in a 5 T field (FC). A low-temperature SIRM was obtained by applying a 5 T field at 5 K. Then ZFC and FC curves were measured in a zero field during warming from 5 to 300 K with a step of 5 K/min.

3. Results

3.1. Age Models

For the past 10 ka, the ages of studied Black Sea sediment cores were determined by correlating Ca/Ti rations to that of cores GeoB7608-1 (Bahr et al., 2005) and GeoB7622-2 (Lamy et al., 2006) dated by AMS ^{14}C from the western Black Sea (Figure 1). In Figure 2, Ca/Ti ratios from the studied cores and the Black Sea stack (Jiabo Liu et al., 2020) follow a similar pattern to that of the cores GeoB7608-1 and GeoB7622-2. The Black Sea stack of Ca/Ti ratio using 100-year bins were derived from X-ray fluorescence (XRF) scanning of 14 Black Sea sediments cores (Ca/Ti ratios of all individual cores refer to the supplementary in Jiabo Liu et al., 2020). The obtained ages are further constrained by an ash layer Z2 at about 3.6 ka (Höflmayer, 2012) identified in cores GeoB7622–2 (Lamy et al., 2006) and M72/5–25GC1 (Cullen et al., 2014). The onset of sapropelic sedimentation at about 8.3 ka (e.g., Badertscher et al., 2011; Bahr et al., 2008; Lamy et al., 2006) is indicated by a greyish bar in Figure 2. More detailed correlations and age depth models of the studied cores are provided by Nowaczyk et al. (2020) for the Holocene and by Jiabo Liu et al. (2020) for the Pleistocene sediments.

3.2. Relict Magnetic Minerals

In studied Black Sea sediments, pyrite framboids with diameters ranging from a few to about dozens of micrometers are commonly found in samples from different depths from core MSM33-55-1 (Figures 3a–3c). After magnetic extraction, relict magnetic minerals of hemoilmenite, Fe-Mn and Fe-Cr spinels, and magnetic inclusions are found in SEM observations (Figure 3d–o). Corresponding EDS spectra results of the relict magnetic crystals are shown in Supporting Information S1. The relative percentage of elements Fe, Ti, Mg, Al, Si, Mn and Cr, and Ti/Fe ratios are shown in Figure S1 in Supporting Information S1. The measured EDS spectra results of samples shown in Figure 3 are characterized by Ti/Fe ratios ranging from 0.4 to 2 which is similar to hemoilmenite (e.g., Dillon & Franke, 2009; Gehring et al., 2008). In addition, minor concentrations of Mn and Mg observed in the EDS spectra of hemoilmenite (Gehring et al., 2008) are also found in raw samples of this study.

In the magnetic extractions, magnetic inclusions hosted in silicates can be found in both SEM (Figure 3j) and TEM observations (Figure 4). In Figure 4, the EDS analyses on the silicate particle indicate peaks of Iron (Fe), Oxygen (O), and Silica (Si; Figure 4c), which is coinciding with that of magnetite inclusions (e.g., Chang, Roberts, et al., 2016; Jiang et al., 2021). In Figures 4b and 4a lattice fringe image is shown for one magnetite inclusion. The diffraction pattern (FFT) of the lattice fringe yields values of 36.0°, 35.0°, 54.5°, and 54.5° between adjacent lattice planes (Figure 4d), which is indicative of magnetite in [01-1] zone axis orientation.

The magnetic inclusions are protected by host silicates and can survive HCL treatment. Jiang et al. (2021) show that sediments dissolved in 10 mol/L HCL solution for 24 hr can efficiently remove biogenic and unprotected magnetic phases and preserve silicate hosted magnetic inclusions. In studied Black Sea sediments, SEM images of magnetic extractions from residuals after HCL treatment indicate the survivals of hemoilmenite skeletons, Cr-Fe spinels, and magnetic inclusions (Figure S2 in Supporting Information S1). Compared to the hemoilmenite particles from untreated sediments (Figure 3), the hemoilmenite skeletons from HCL treated residuals

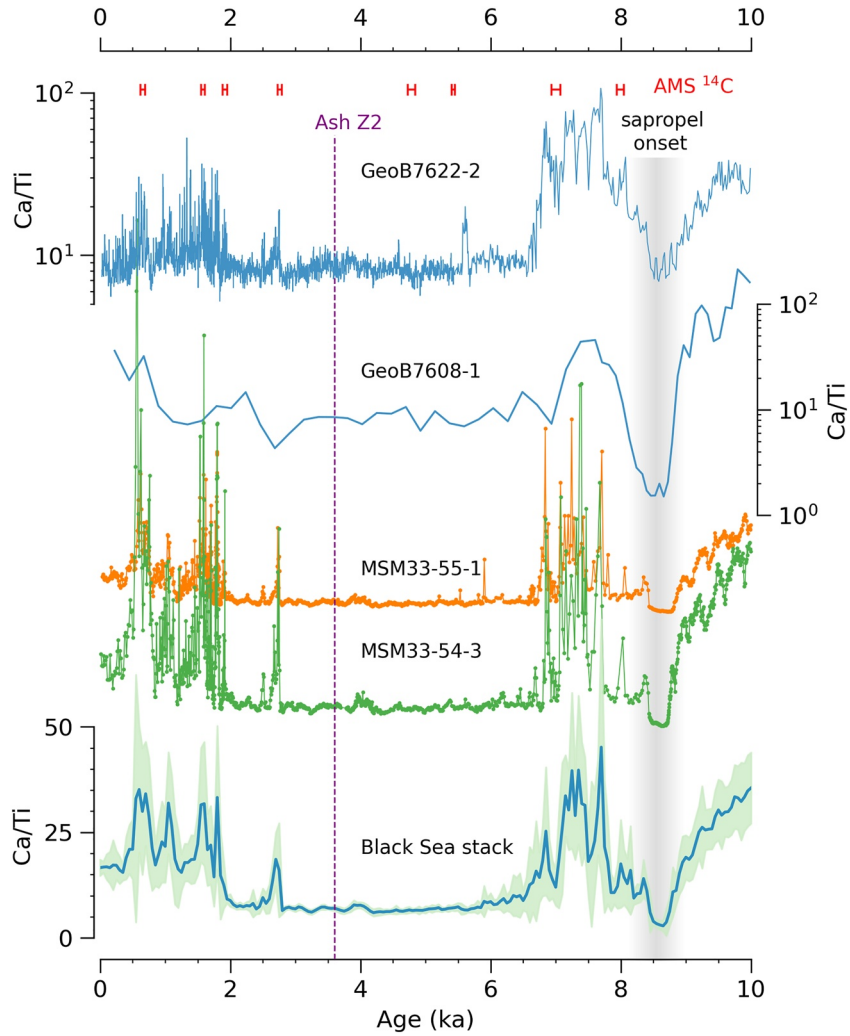

Figure 2. Ages of cores MSM33-55-1 and MSM33-54-3 for the Holocene period (0-10 ka) are determined by correlating Ca/Ti ratios to those of cores GeoB7608-1 (Bahr et al., 2005) and GeoB7622-2 (Lamy et al., 2006) from the western Black Sea (Figure 1). The AMS ^{14}C ages with 1σ error bars from core GeoB7622-2 are shown on the top. The Black Sea stack of Ca/Ti ratio (Jiabo Liu et al., 2020) is plotted with 1σ standard deviation band. The ash Z2 indicates the Minoan Santorini eruption at about 3.6 ka (Höflmayer, 2012). The start of the sapropelic sedimentation in the Black Sea is marked by a gray bar at about 8.3 ka (e.g., Kwiecien et al., 2008; Major et al., 2006).

are characterized by holes and cracks (Figure S2 in Supporting Information S1). Additionally, EDS spectra results indicate that Ti/Fe ratios are getting slightly higher after HCL treatment (Figure S1b in Supporting Information S1).

With respect to the untreated samples, the residuals after HCL treatment from two Black Sea sediment samples exhibit significant decrease in magnetization (Figure 5 and Table 1). About half weight of the studied samples were left after the HCL treatment, but the residuals of the two samples only account for 13.4% and 22.0% of the total SIRM (Table 1). Thus, it is very likely that the observed holes and cracks in hemoilmenite skeletons under SEM (Figure S2 in Supporting Information S1) from HCL treated residuals were occupied by other ferrimagnetic minerals. Note the hysteresis curves were corrected to better observe the components from ferrimagnetic contributions (Figure 5b). The raw hysteresis loops (Figure 5a) indicate strong linear response of magnetic moment (M) to the applied field (B) before and after the dissolution, which is due to substantial contributions of the paramagnetic pyrite and silicates.

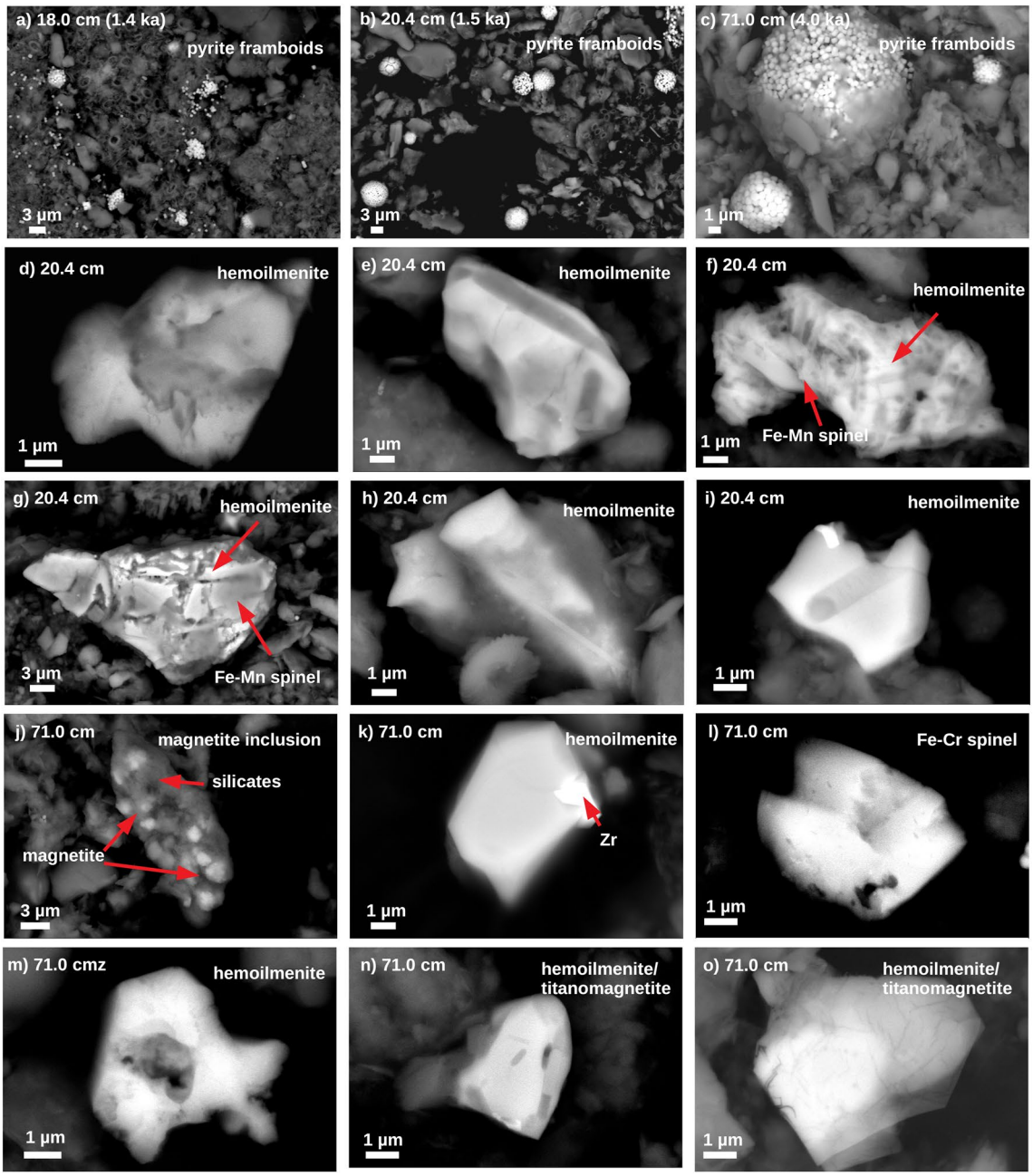

Figure 3. Scanning electron microscope (SEM) images, backscatter mode, of (a–c) bulk sediments and (d–o) magnetic extractions from core MSM33-55-1. (a–c) Pyrite framboids are pervasive in bulk sediments. (d–o) Relict magnetic minerals are mainly hemoilmenite, Fe-Mn and Fe-Cr spinels, and magnetite inclusions. Corresponding energy-dispersive X-ray spectroscopy (EDS) data of crystals from (e-o) are shown in Supporting Information.

3.3. Rock Magnetic Properties

In Figure 6, detailed rock magnetic results exhibit comparable patterns among four bulk samples selected from core MSM33-55-1. Temperature-dependent κ_{LF} curves (κ-T) in Figure 6a display very low values during heating (red curve), whereas remarkably high values during cooling (blue curve) after about 580°C, which denotes the formation of magnetite after heating. Due to the abundant pyrite framboids in studied samples, the pattern of κ-T curves is mainly caused by the thermochemical alteration of pyrite. In the right column of Figure 6a, low-temperature FC-ZFC curves are shown for the magnetic extraction sample from 4.8 ka. During warming, the ZFC curve exhibit a minimum at about 12 K and then a steep increase with a peak at about 40 K. The FC curve shows a

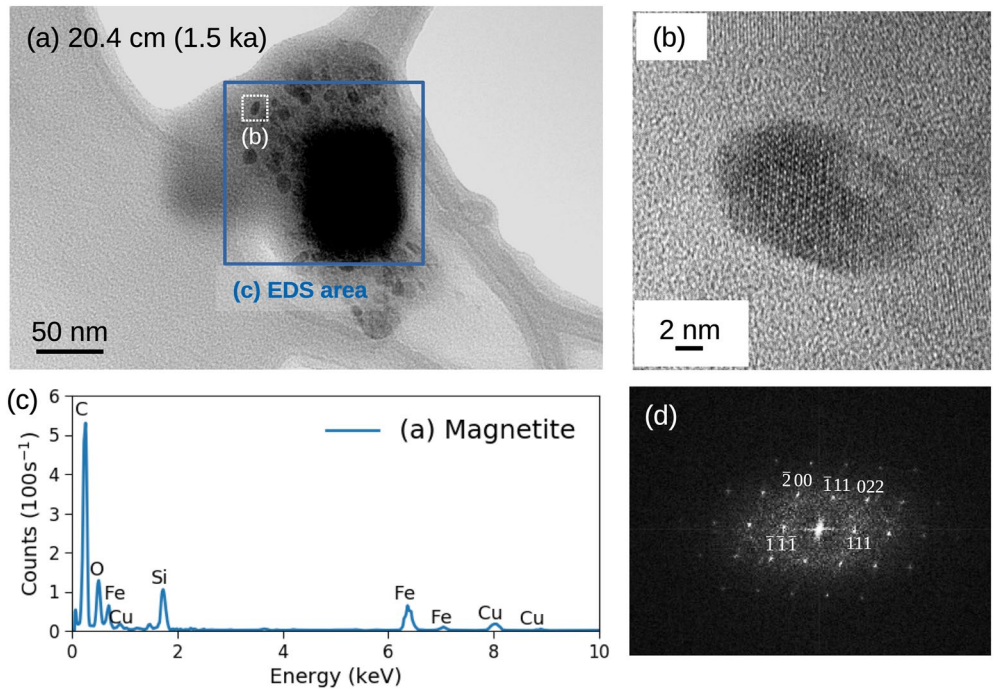

Figure 4. Transmission electron microscope (TEM) analyses of one magnetic inclusion bearing silicate from core MSM33-55-1. (a) Bright-field TEM image of the silicate particle. (b) Lattice fringe image of an inclusion inside the silicate. (c) EDS spectrum of the host silicate. (d) The diffraction pattern (fast Fourier transform, FFT) of the inclusion shown in (b).

sharp decrease between 5 and 12 K. The ZFC curve of studied sample is similar to that of hemoilmenite particles (Gehring et al., 2008), though the FC-ZFC curve reported by Gehring et al. (2008) was measured with a direct current filed of 10 mT. Gehring et al. (2008) suggested that the peak of FC-ZFC at about 45 K is due to the onset of spin glass-like states in the hemoilmenite.

In Figure 6b, IRM acquisition curves are decomposed into three components based on different magnetic mineral coercivities. In all studied samples, the dominant components plotted as red lines contribute to more than 80% of the total IRM. Besides, the dominant components are characterized by a narrow distribution (dispersion parameter = 0.18–0.19) and low median field (20–25 mT), which are generally related to magnetite (e.g., He et al., 2020). The irFORC (Figure 6c) and tfFORC (Figure 6d) diagrams are used to indicate the domain states of magnetic minerals. The irFORC distributions of studied samples have a positive peak along the B_c axis up to ~50 mT and spreading the $B_i > 0$ axis up to ~30 mT, and a negative region along the $B_i < 0$ axis. This pattern is typically found in samples bearing SD magnetite (e.g., Chang, Roberts, et al., 2016; Jiang et al., 2021). The tfFORC diagrams also show positive peaks along the B_c axis (Figure 6d) which are also a key indicator of the presence of SD particles (Zhao et al., 2017). In addition to magnetic inclusions, the ferrimagnetic minerals hosted in hemoilmenite should be responsible for the measured low magnetic coercivities and SD behavior.

3.4. Paleomagnetic Results

Detailed AF demagnetization graphs of selected samples from cores MSM33-55-1 and MSM33-54-3 spanning the past 9 ka are shown in Figure 7. For all samples, vector end-points migrate straight to the origin, with only minor vicious magnetization removed during the first AF step (Figure 7). ChRM directions, inclinations in red, and declinations in blue are generally determined between AF steps of 30 and 50 mT. The derived inclinations are slightly shallower than the expected inclination of 61° (red dashed line) calculated from a geocentric axial dipole field. Without horizontal directional information during coring, declinations are adjusted to a mean value of 0° for every individual cores. In NRM decay curves, the NRM intensities are generally decreasing to zero after the AF step of 50 mT. Additionally, gyro-remanent magnetization (GRM), which is typically found in greigite bearing samples (e.g., Ebert et al., 2021; Nowaczyk et al., 2020), is not observed in the studied samples.

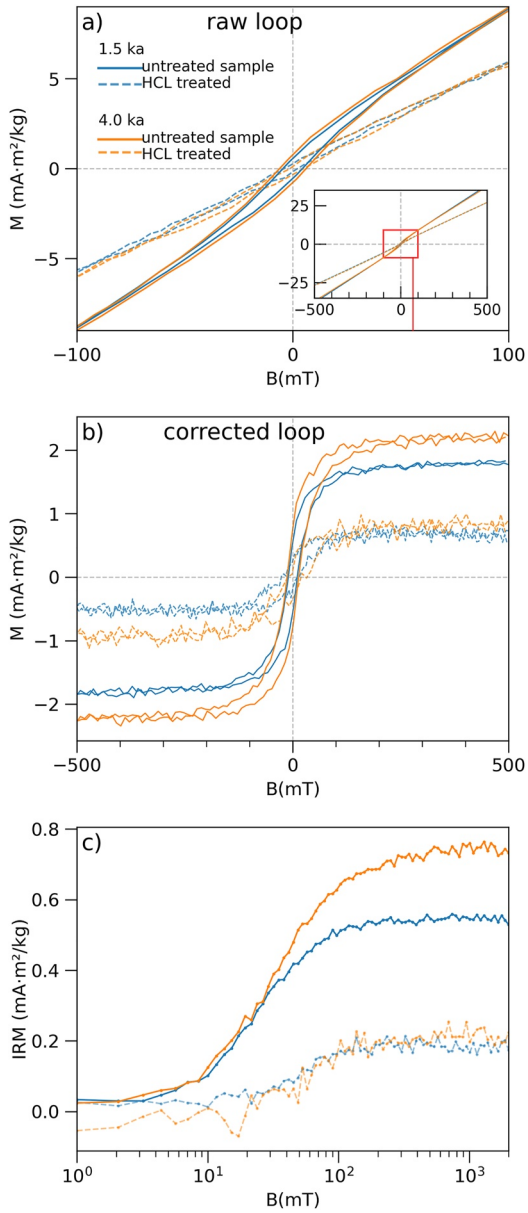

Figure 5. Rock magnetic properties of the untreated sediments and HCL treated residuals from core MSM33-55-1. (a) Raw hysteresis loops. (b) Corrected hysteresis loops for ferrimagnetic minerals. (c) Isothermal remanent magnetization (IRM) acquisition curves.

Table 1
Summary of the Magnetic Characteristics of HCL Treated Residuals From Core MSM33-55-1

Age (BP)	Depth in core (cm)	Mass fraction (wt%)	SIRM (mA·m²/kg)	SIRM fraction (%)
1.5 ka	20.4	46.8	1.07	13.4%
4.0 ka	71.0	55.1	1.82	22.0%

Note. The fractions of mass and saturated isothermal remanent magnetization (SIMR) are in proportion to the original untreated samples.

In Figure 8, the paleo- and rock magnetic results recorded by the relict magnetic minerals for the past 8 ka are plotted together with the previous published datasets for the 8–30 ka interval (Jiabo Liu et al., 2019; Nowaczyk et al., 2018). Before ~14 ka, the Black Sea sediments are dominated by detrital (titano-)magnetite minerals with sporadically formed greigite, mostly in micro-environments. The greigite bearing samples, indicated by SIRM/κ_{LF} ratios >10 kAm^{-2} (Nowaczyk et al., 2012, 2020) are plotted as empty gray symbols. In sediments deposited between about 14 and 8 ka, greigite and pyrite were formed in sediments because of the seawater penetration from overlying sediments after the seawater ingression (e.g., Neretin et al., 2004; Strechie et al., 2002). In Figure 8a, the decrease of κ_{LF} after about 14 ka is due to the successive dissolution of detrital (titano-)magnetite and the subsequent formation of paramagnetic pyrite. With respect to greigite and/or (titano-) magnetite samples from 8 to 30 ka, the relict magnetic minerals from 0 to 8 ka are characterized by very low κ_{LF} and remarkably high ARM/SIRM values, indicating smaller grain sizes. Note that the κ_{LF} amplitudes in the 0–8 ka interval are strongly influenced by the presence of paramagnetic pyrite framboids and silicates which may also bias the SIRM/κ_{LF} ratios. Between 8 and 20 ka, rock magnetic properties of the studied cores are severely affected by secondary ferrimagnetic greigite which can also compromise paleomagnetic results. Thus, we only compare the relict magnetic mineral samples from 0 to 8 ka to the (titano-)magnetite samples from 20 to 30 ka.

In Figure 9, the paleointensity and inclination recorded by relict magnetic mineral samples from 0 to 8 ka are compared to those of (titano-)magnetite samples from 20 to 30 ka, and to predictions from the model GGF100k (Panovska et al., 2018) at the Black Sea site (42°N, 37°E). For this study, the RPI stacked from 16 Black Sea cores (BS stack, Jiabo Liu et al., 2020; Nowaczyk et al., 2013) covering the interval 20–30 ka was scaled to the intensity F predicted from the GGF100k model, following $F = 20 + \text{RPI}*66.67$. The same protocol is applied to the RPI from cores MSM33-55-1 and MSM33-54-3 (Figures 9a and 9b). The mean field intensities F ($\overline{F}$) with 1σ distribution from the studied records and the GGF100k are shown for the 0–8 ka (left panel) and the 20–30 ka (right panel) intervals in Figure 9e and listed in Table 2. For 20–30 ka, the $\overline{F}$ amplitudes of the BS stack exhibit distributions similar to the GGF100 ka (Figure 9e), which denotes a reasonable conversion from RPI values to absolute F amplitudes. Based on the GGF100k model, the predicted F amplitudes at the Black Sea site are generally higher and more variable during 0–8 ka than during 20–30 ka (Figure 9e). Although with slightly different $\overline{F}$ values, the two studied cores show comparable $\overline{F}$ values and 1σ distributions with the GGF100k for the 0–8 ka, as well as for the 20–30 ka. The inclinations of studied cores show identical amplitudes between the 0–8 ka (Figure 9f) and the 20–30 ka (Figure 9g) intervals. Without validated excursion events in the discussed time windows, the mean inclinations (~55°) of studied cores slightly deviate from the expected inclination (~61°) from a geocentric axial dipole field. The inclination shallowing factor *f* followed Bilardello and Kodama (2010) are 0.80 and 0.78 for the 0–8 ka and the 20–30 ka intervals, respectively.

4. Discussion

In the modern Black Sea, when traveling through the water column, detrital magnetic minerals are dissolved, subsequently forming pyrite framboids driven by SO_4-AOM (Jørgensen et al., 2004; Peckmann et al., 2001; Raiswell

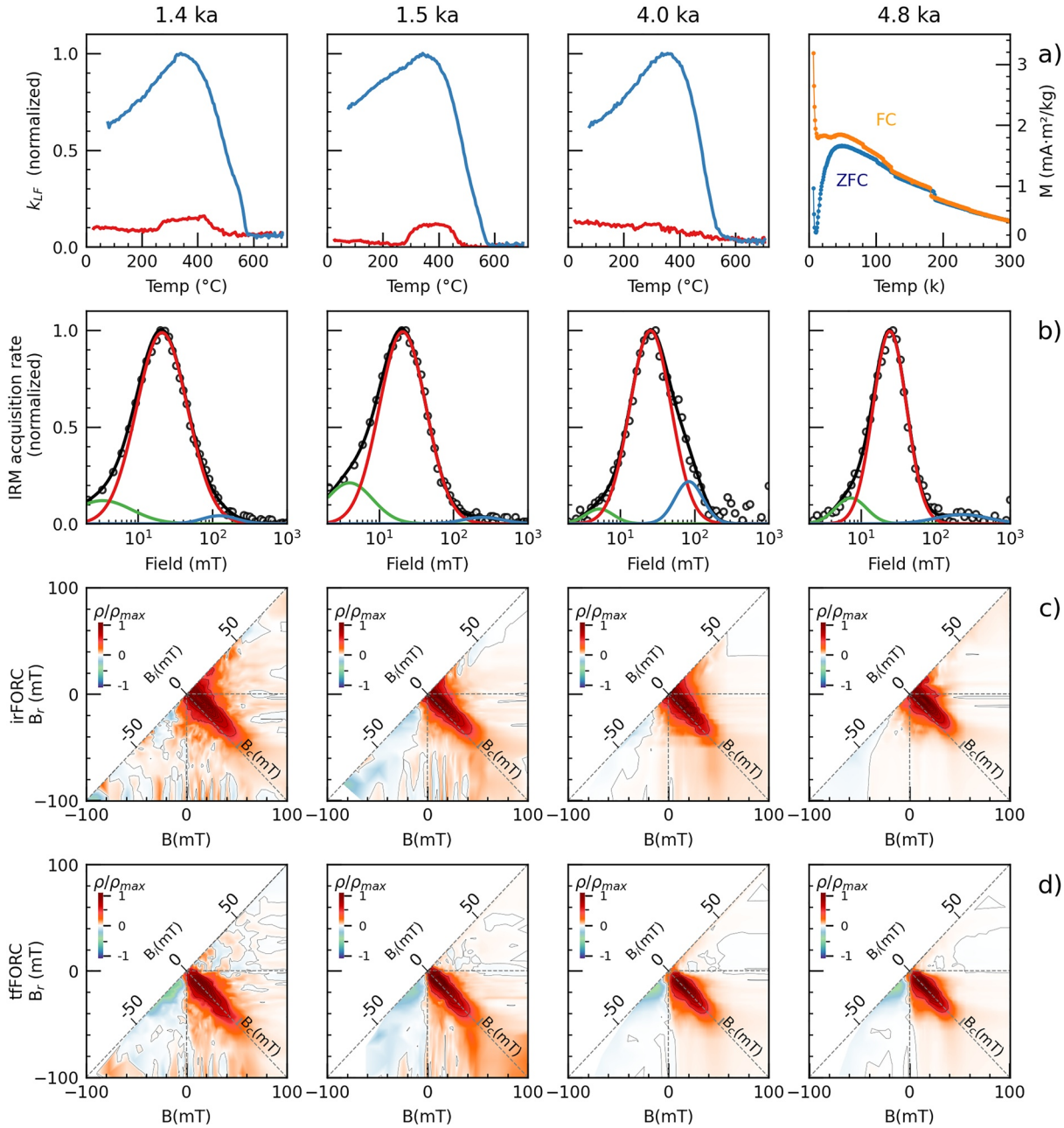

Figure 6. Rock magnetic results of samples from core MSM33-55-1. (a) Temperature-dependent κ_{LF} curves plotted with heating curves in red and cooling curves in blue. In the right column, low-temperature SIRM warming curves are shown for one sample. (b) IRM acquisition curves plotted with hollow circles are decomposed into three components indicated by green, red, and blue lines. (c) irregular FORC (irFORC) and (d) transient hysteresis-free FORC (tfFORC) diagrams were calculated with a smooth factor (SF) of 3 and their distributions ρ were normalized by their respective maximum ρ_{max}. κ_{LF} - magnetic susceptibility; (S)IRM - (saturated) isothermal remanent magnetization; FORC- first order reversal curve.

& Canfield, 1998; Riedinger et al., 2017). The pyrite framboids are pervasive in studied Black Sea sediments covering the past 8 ka (Figure 3), but the paramagnetic pyrite does not carry a permanent magnetic remanence. In the studied Black Sea sediments, it is found that the relict hemoilmenite with ferrimagnetic minerals, Fe-Cr and Fe-Mn spinels, and magnetic inclusions are the magnetic carriers.

The ability of recording a DRM by relict magnetic minerals, specifically the magnetic inclusions, have been increasingly investigated recently since they are resistant to diagenesis. Besides, the magnetic inclusions in marine sediments are commonly reported as SD or vortex state size range (Chang et al., 2016; Jiang et al., 2021) and can

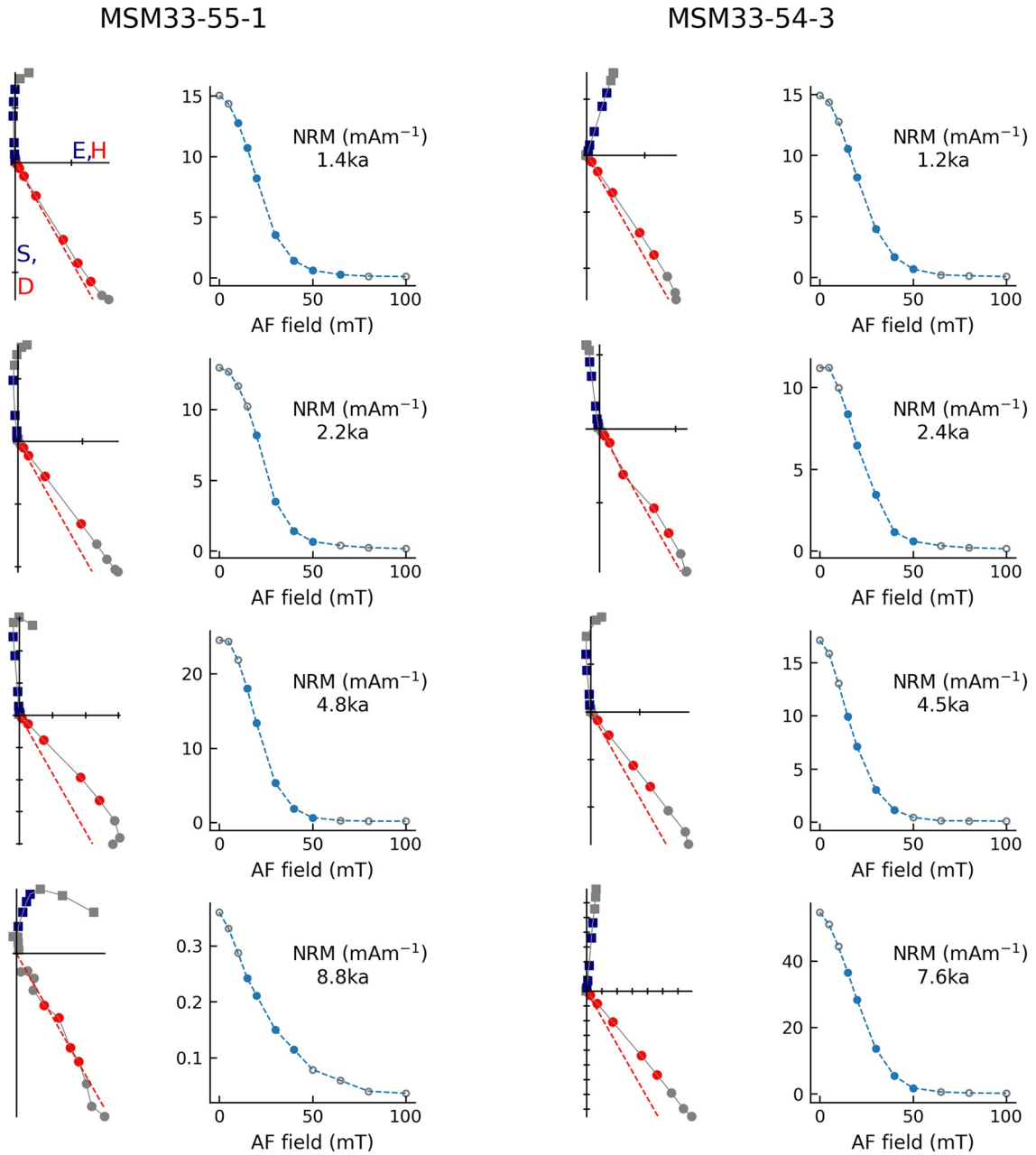

Figure 7. Alternating Field (AF) demagnetization results of samples from cores MSM33-55-1 (left panel) and MSM33-54-3 (right panel) spanning the past 9 ka. In vector endpoint diagrams, square and circle symbols indicate data in East versus South plane and Horizontal versus Down plane, respectively. The symbols in blue and red colors denote data used to determine characteristic (ChRM) directions. The red dashed line indicates the inclination of 61° at the study site expected from a geocentric axial dipole field. The declinations are shown after corrected to a mean value of 0° for individual cores. In natural remanent magnetization (NRM) decay curves, solid circles denote the AF steps of ChRM determinations.

significantly contribute to the paleomagnetic signals (Chang et al., 2021; Hong et al., 2019). The DRM recorded by magnetic inclusions is strongly dependent on the size of host silicate minerals (Chang et al., 2021). Magnetic inclusions hosted in larger host silicates have a weaker response to a geomagnetic torque than small particles, which leads to lower paleomagnetic recording efficiency compared to biogenic magnetite and other detrital magnetic minerals (Chen et al., 2017; Hong et al., 2019). In contrast, the hemoilmenite and iron spinels carry only a weak magnetization. In the anoxic sediments from the Niger deep-sea fan, Dillon and Franke (2009) suggested that (titano-)magnetite is most likely replaced by paramagnetic iron sulfide, and ilmenite–hematite solid solution series are the prevailing contributor to the magnetization. The abundant hemoilmenite and iron spinels are also

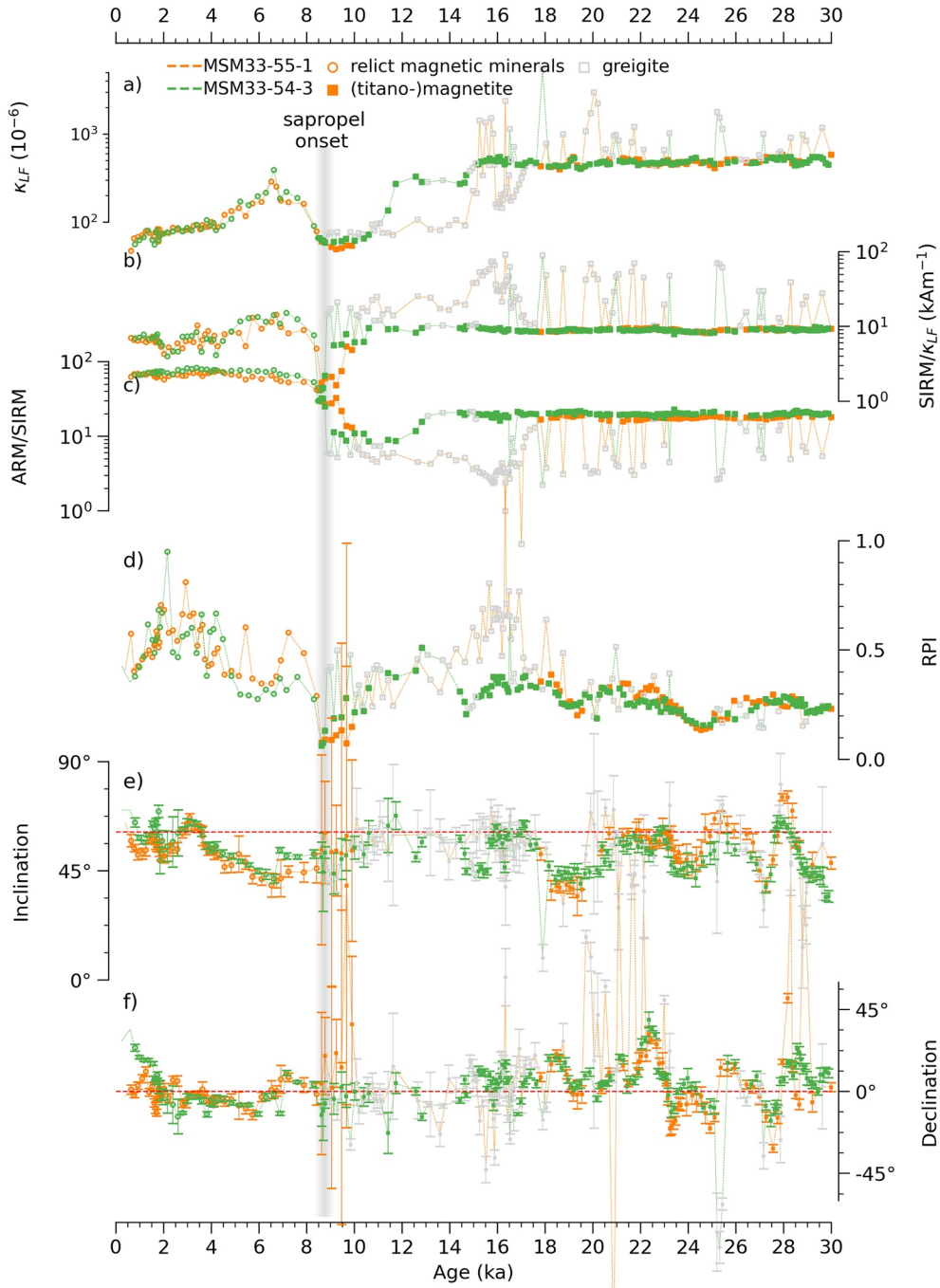

Figure 8. Paleo- and rock magnetic results from cores MSM33-55-1 and MSM33-54-3 spanning the past 8 ka (this study) compared to those from 8 to 30 ka (Jiabo Liu et al., 2019; Nowaczyk et al., 2018). (a) Magnetic susceptibility κ_{LF} implies the bulk content of magnetic minerals. (b) SIRM/κ_{LF} ratios >10 kAm^{-1} are indicative of greigite bearing samples in the glacial Black Sea sediments. (c) High ARM/SIRM ratios denote fine sized magnetic minerals. (d) Relative paleointensity (RPI) is determined by the slope between NRM and ARM. Directions of (e) inclination and (f) declination are plotted with α_{95} uncertainties. The horizontal dotted lines in inclination (61°) and declination (0°) are the expected directions from a geocentric axial dipole field at the study site. ARM - anhysteretic remanent magnetization.

found in the studied anoxic Black Sea sediments (Figure 3). The HCL dissolution experiments revealed that the dissolved ferrimagnetic minerals hosted in the holes and cracks of hemoilmenite skeletons likely account for high fractions (~80%, Table 1) of the total SIRM. In addition, the magnetic properties of the Black Sea sediments

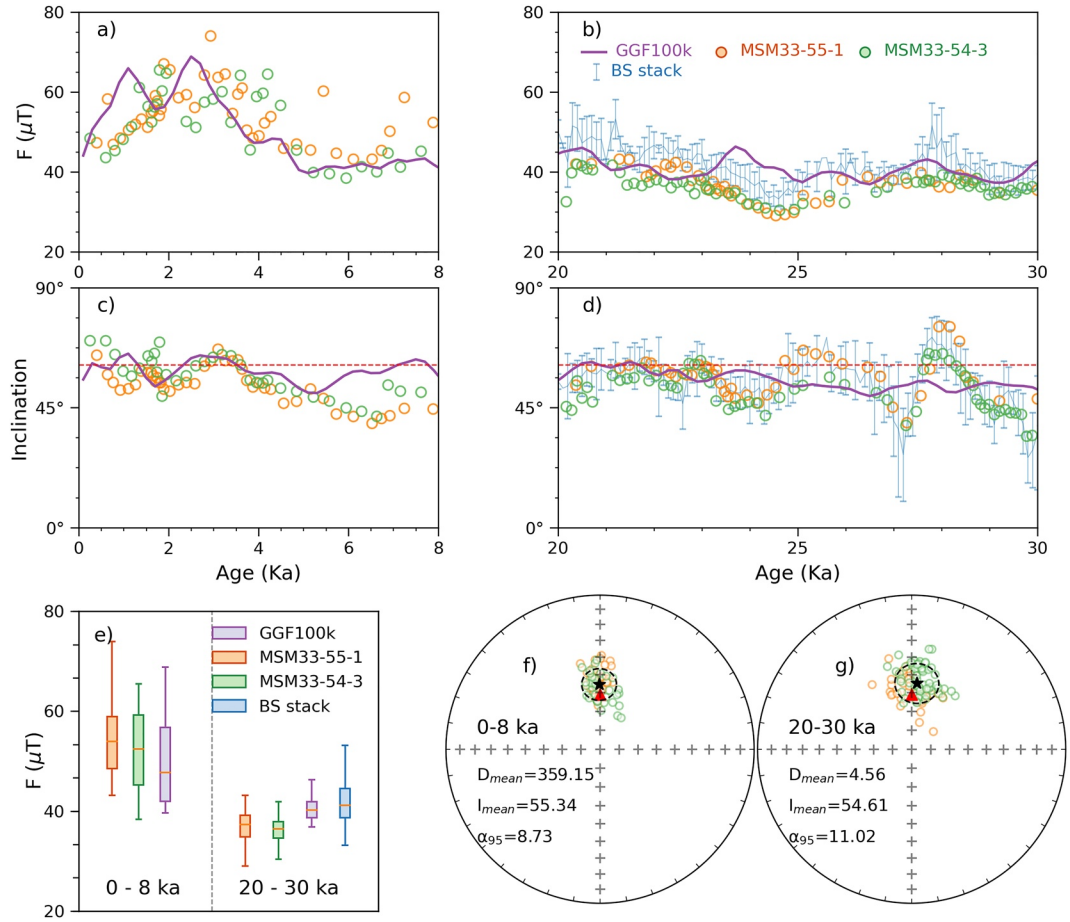

Figure 9. Comparison of the Holocene (0–8 ka) and the last glacial (20–30 ka) paleosecular variations from cores MSM33-55-1 and MSM33-54-3. (a) and (b) Intensity F of studied cores and the Black Sea stack (BS stack, Liu et al., 2020) aligned to the referenced F predicted from the GGF100k model (Panovska et al., 2018). (c) and (d) Inclination curves shown together with a horizontal dashed line of the dipole inclination of 61°. (e) Comparison of mean F ($\overline{F}$) of the Black Sea record and that of the GGF100k field models for 0–8 ka and 20–30 ka intervals (also list in Table 2). (f) and (g) show the Fisher statistics of paleomagnetic directions from the Black Sea cores. The black stars and dotted circles mark the mean direction and its α_{95} uncertainty, respectively. The red triangle indicates the direction of a geocentric axial dipole field.

are characterized by SD behavior and low magnetic coercivities (Figure 6), which likely represent the magnetic inclusions and the ferrimagnetic minerals hosted in hemoilmenite particles.

Data from studied Black Sea cores show that the field intensity F_{BS} derived from relict magnetic mineral samples (0–8 ka) are comparable to the values derived from (titano-)magnetite samples (20–30 ka), indicating that both

Table 2
Summary of Mean Field intensity F of the Converted Black Sea RPI Record ($\overline{F}_{BS}$) and the Predicted F From GGF100k ($\overline{F}_{GGF}$) Field Model (Panovska et al., 2018) for the Holocene (0–8 ka) and the Last Glacial (20–30 ka) Periods

Time interval	Magnetic carriers	Core	$\overline{F}_{BS}$ (μT)	$\overline{F}_{GGF}$ (μT)	$\overline{F}_{BS}/\overline{F}_{GGF}$
0–8 ka	Relict magnetic minerals	MSM33-55-1	54.33	50.13	1.08
		MSM33-54-3	52.87		1.05
20–30 ka	(titano-)magnetite particle	MSM33-55-1	36.80	40.55	0.91
		MSM33-54-3	36.27		0.89
		Black Sea stack	41.73		1.03

Note. RPI - relative paleointensity.

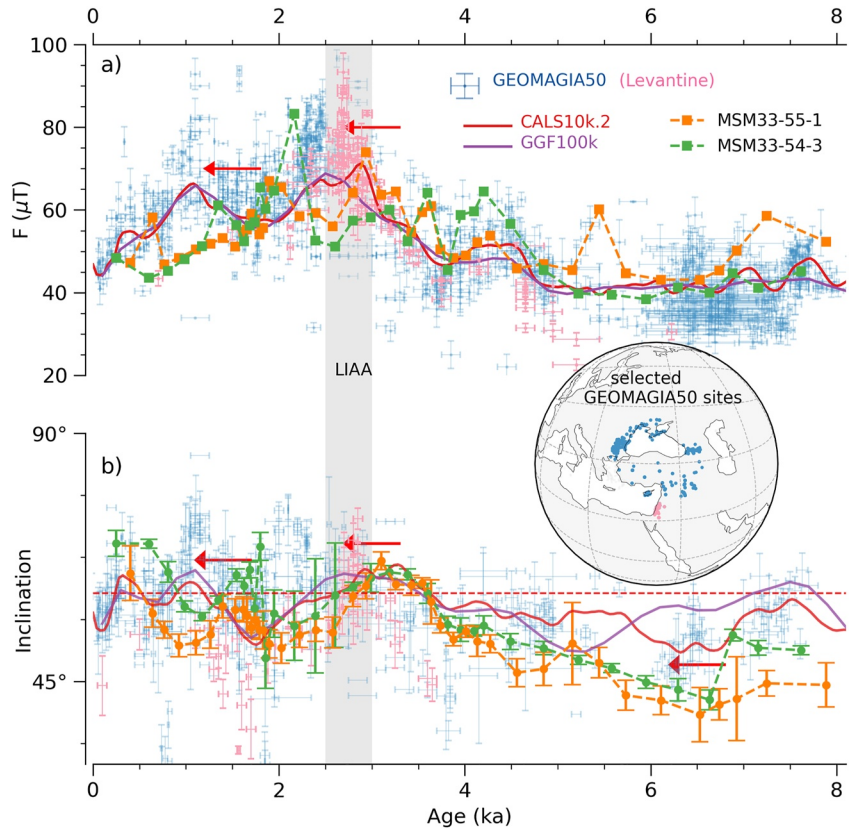

Figure 10. (a) The field intensity (f) and (b) inclination reconstructed from two Black Sea cores compared to regional and global records for the past 8 ka. The volcanic and archeomagnetic datasets from GEOMAGIA50 (Brown et al., 2015) are shown in blue for sites inside the 10° circle around the Black Sea site (42°N, 37°E), and in pink for sites from the Levant region. The F and inclination at the study site predicted from models of GGF100k (Panovska et al., 2018) and CALS10k.2 (Constable et al., 2016) are shown by solid purple and red lines, respectively. The Levantine Iron Age Anomaly (LIAA) firstly reported from the Levant region (Shaar et al., 2016) is marked by a gray bar.

types of remanence carriers can reproduce the features of F_{GGF} predicted from the data-constrained GGF100k field model (Figure 9e). With respect to the 20–30 ka interval, the $\overline{F}_{BS}/\overline{F}_{GGF}$ ratio shows higher values for the 0–8 ka (Table 2). This is likely due to the different efficiencies in recording the DRM between relict magnetic minerals and (titano-)magnetite minerals. Nevertheless, the inclinations from 0 to 8 ka and 20–30 ka intervals have identical mean values (~55°) and shallowing factors (f = ~0.79). Besides, the shallowing factor of studied cores are similar to that of natural magnetite-bearing samples (f = 0.54–0.79; Bilardello & Kodama, 2010). Although the efficiency of the studied relict magnetic mineral assemblage in recording the DRM is not yet known, the paleo- and rock magnetic results indicate they are comparable to other detrital (titano-)magnetite and are able to properly record the paleomagnetic field variations.

The derived records of F and inclination from cores MSM33-55-1 and MSM33-54-3 covering the past 8 ka also resemble comparable patterns with those of the GEOMAGIA50 datasets (Brown et al., 2015) and the predictions from the CALS10k.2 (Constable et al., 2016) and GGF100k (Panovska et al., 2018) field models (Figure 10). Nevertheless, an apparent time lag of about 0.5 ka of the studied Black Sea PSV records can be observed, which we attribute to the effect of lock-in depth of the PDRM (e.g., Roberts & Winklhofer, 2004). The studied sediments are characterized by mean sedimentation rates of about 10.75 cm/kyr and 12.6 cm/kyr in the past 8 ka. Due to progressive sediment consolidation and dewatering, the DRM was probably locked in about 5 cm (equivalent to about 0.5 ka) below the surface mixed layer. The time lag of about 0.5–0.7 ka was further confirmed by a cross-correlation analysis between the studied Black Sea records and the GGF100k model (Figure S3 in Supporting Information S1). By shifting the data from the studied cores to 0.5 ka younger ages, indicated by red arrows in Figure 10, the obtained records of F and inclinations become congruent with the predictions of the CALS10k.2

and the GGF100k field models. In contrast to the GEOMAIGA datasets, F and inclination of this study exhibit weaker variable fluctuations which is interpreted to result from sedimentation rates and lock-in effects.

The most prominent feature of the Holocene geomagnetic field at the Mediterranean region is the LIAA at about 3 ka BP (Shaar et al., 2016). At the Levant region, the LIAA exhibited high field intensity and large directional deviations (Ben-Yosef et al., 2009; Shaar et al., 2016). With an offset of about 0.5 ka, the LIAA is characterized by moderate peaks of F and inclination in the Black Sea records. For one reason, the studied Black Sea records are smoothed. For another, the intense flux patche associated with the LIAA was growing and decaying mostly restricted to the Levant region (Korte & Constable, 2018), thus the extremely high intensity was not observed at the Turkey-Georgia area (Rivero-montero, Gómez-Paccard, Kondopoulou, et al., 2021), close to the coring sites of this study.

The Black Sea data also exhibit a peak of intensity and a large shift of inclination at about 1.8 ka. After shifting about 0.6 ka indicated by red arrows, this pattern can be correlated with the high intensity feature at about 1.2 ka BP which are commonly found at Europe (Genevey et al., 2016). In high-resolution archeomagnetic datasets mainly from central Europe and the Balkan Peninsula, the high intensity feature exhibit two peaks and is regarded as a double-oscillation at about 1.2 ka (Kovacheva et al., 2014; Rivero-Montero, Gómez-Paccard, Pavón-Carrasco, et al., 2021). But from Iberian Peninsula and east Europe (Rivero-montero, Gómez-Paccard, Kondopoulou, et al., 2021), the double-oscillation is not well recognized and the intensity curves indicate a single peak which is alike the studied Black Sea record. Nevertheless, the Black Sea records only have limited temporal resolution, to identify the double-oscillation feature at the Black Sea area needs future work yielding high-resolution PSV records.

Another noteworthy feature of the Black Sea PSV record is the lowest inclination at bout 6.5 ka. Between 7 ka and 5 ka, the inclinations of Black Sea records are much shallower than that of the CALS10k.2 and the GGF100k models, though they exhibit consistent intensity lows for this time interval. The directional data from GEOMAGIA50 database are fairly sparse for the 7–5 ka period. Nonetheless, with a shift of 0.5 ka, the shallowest inclinations of the Black Sea records can be overlapped with the GEOMAGIA50 datasets at bout 6 ka. Besides, shallow inclinations centered at about 6.5 ka BP are also observed in archeomagnetic results from Bulgaria (Kovacheva et al., 2014). Thus, we infer that the shallow inclinations at about 6.5 ka in the studied Black Sea records are true features of the paleomagnetic field.

Though hampered by limited temporal resolution, the obtained paleomagnetic results from the Holocene anoxic Black Sea sediments represent reliable paleomagnetic variations which resembled the LIAA and other features of high intensity and steep inclinations in the past 8 ka. Our study demonstrates that it is possible to recover reliable paleomagnetic results from anoxic sediments. A major issue of investigating the Earth's magnetic field is unevenly distributed paleomagnetic data (Panovska et al., 2019). Changing redox water conditions of bottom water following climate variations on all time scales, can lead to magnetic mineral diagenesis in sediments and bias the DRM record. Especially during warm periods, for example, the most recent Holocene, general high input of organic matters turned lakes, marginal seas, and continental shelves into sub-/an-oxic water environments (e.g., Björck, 1995; Jianxing Liu et al., 2014; Wegwerth et al., 2018). The relict magnetic minerals are widely existing and resist to reductive dissolution under sulphidic conditions (Chang et al., 2016; Hounslow, 1996; Hounslow et al., 1995; Nowaczyk, 2011; Wilson & Roberts, 1999). Thus, they are potential targets of future paleomagnetic studies in various reducing geological realms.

5. Conclusions

This study evidenced that relict ferrous hemoilmenite, Fe-Cr and Fe-Mn spinels, and magnetic inclusions are the magnetic carriers in the Holocene Black Sea sediments deposited under anoxic bottom water conditions. We could show that the DRM recorded by the relict magnetic minerals is comparable to that recorded by detrital (titano-)magnetite samples in two Black Sea sediment cores. Moreover, the PSV derived from the two Black Sea cores reliably recorded the dynamic patterns of the regional geomagnetic field for the past 8 ka as predicted by data-based field models. Thus, this study demonstrate that carefully performed future paleomagnetic studies on sediments from various marginal seas, continental shelves, and lakes with reducing bottom-water condition can contribute to analyses of global geomagnetic field dynamics over geological time.

Data Availability Statement

Standard rock magnetic data from all investigated cores taken during expedition M72/5 of German *RV Meteor* are available via GFZ Data Services, Nowaczyk et al. (2021a), https://doi.org/10.5880/GFZ.4.3.2021.002. Standard rock magnetic data from all investigated cores taken during expedition MSM33 of German *RV Maria S. Merian* are available via GFZ Data Services, Nowaczyk et al. (2021b), https://doi.org/10.5880/GFZ.4.3.2021.003.

Acknowledgments
We thank S. Plewe and Han Peng for their help with SEM operating at the IOW and the SUSTech, respectively, A. Schreiber for TEM sample preparation at the GFZ, B. Klemke for help with MPMS measurements at the HZB, and S. Plewe, M. Duwe, T. Moldenhawer, and F. Brendel for their technical and logistical help during processing and sub-sampling of the cores. We appreciate L. Chang and an anonymous reviewer for their comprehensive comments. We also thank the captain and crews of *RV Meteor* cruise M72/5 and *RV Maria S. Merian* cruise MSM33, for their efforts in providing optimal scientific working conditions. This work was partly funded by the German Research Foundation (Deutsche Forschungsgemeinschaft, DFG SPP 1266 "INTERDYNAMIC" grants AR 367/9-1 and AR 367/9-2), the Gary Comer Science and Education Foundation, U.S.A. J. Liu was supported by the Chinese Scholarship Council (CSC Grant No. 201506180060) for PhD at the GFZ, Germany, and is funded by the China Postdoctoral Science Foundation (2020M682770), the National Natural Science Foundation of China (Grands 42104068, 41874078, 42176066, 92158208), the opening foundations of the Key Laboratory of Marine Geology and Metallogeny, MRN, (No. MGM202003) and the State Key Laboratory of Marine Geology, Tongji University (No. MGK202102) for post-Doctoral researching at the SUSTech, China. J. Liu and Q. Liu is also supported by the Shenzhen Science and Technology Program (KQTD20170810111725321), the opening foundation (SSKP202101) of the Shanghai Sheshan National Geophysical Observatory, Shanghai, China.

References

Badertscher, S., Fleitmann, D., Cheng, H., Edwards, R. L., Gokturk, O. M., Zumbuhl, A., et al. (2011). Pleistocene water intrusions from the Mediterranean and Caspian seas into the Black Sea. *Nature Geoscience*, *4*(4), 236–239. https://doi.org/10.1038/ngeo1106

Bahr, A., Lamy, F., Arz, H., Kuhlmann, H., & Wefer, G. (2005). Late glacial to Holocene climate and sedimentation history in the NW Black Sea. *Marine Geology*, *214*(4), 309–322. https://doi.org/10.1016/j.margeo.2004.11.013

Bahr, A., Lamy, F., Arz, H. W., Major, C., Kwiecien, O., & Wefer, G. (2008). Abrupt changes of temperature and water chemistry in the late Pleistocene and early Holocene Black Sea. *Geochemistry, Geophysics, Geosystems*, *9*(1). https://doi.org/10.1029/2007GC001683

Béguin, A., Filippidi, A., De Lange, G. J., & De Groot, L. V. (2019). The evolution of the Levantine iron age geomagnetic anomaly captured in Mediterranean sediments. *Earth and Planetary Science Letters*, *511*, 55–66. https://doi.org/10.1016/j.epsl.2019.01.021

Ben-Yosef, E., Tauxe, L., Levy, T. E., Shaar, R., Ron, H., & Najjar, M. (2009). Geomagnetic intensity spike recorded in high resolution slag deposit in Southern Jordan. *Earth and Planetary Science Letters*, *287*(3–4), 529–539. https://doi.org/10.1016/j.epsl.2009.09.001

Berner, R. A. (1984). Sedimentary pyrite formation: An update. *Geochimica et Cosmochimica Acta*, *48*(4), 605–615. https://doi.org/10.1016/0016-7037(84)90089-9

Bilardello, D., Jezek, J., & Gilder, S. A. (2013). Role of spherical particles on magnetic field recording in sediments: Experimental and numerical results. *Physics of the Earth and Planetary Interiors*, *214*, 1–13. https://doi.org/10.1016/j.pepi.2012.10.014

Bilardello, D., & Kodama, K. P. (2010). Rock magnetic evidence for inclination shallowing in the early Carboniferous Deer Lake Group red beds of Western Newfoundland. *Geophysical Journal International*, *181*(1), 275–289. https://doi.org/10.1111/j.1365-246X.2010.04537.x

Björck, S. (1995). A review of the history of the Baltic Sea, 13.0-8.0 ka BP. *Quaternary International*, *27*(C), 19–40. https://doi.org/10.1016/1040-6182(94)00057-C

Brown, M. C., Donadini, F., Korte, M., Nilsson, A., Korhonen, K., Lodge, A., et al. (2015). GEOMAGIA50.v3: 1. General structure and modifications to the archeological and volcanic database. *Earth Planets and Space*, *67*(1), 83. https://doi.org/10.1186/s40623-015-0232-0

Cai, S., Doctor, R., Tauxe, L., Hendrickson, M., Hua, Q., & Leroy, S. (2021). Archaeomagnetic results from Cambodia in Southeast Asia: Evidence for possible low-latitude flux expulsion. *Proceedings of National Academy of Sciences of United States of America*, *118*(11), 1–7. https://doi.org/10.1073/pnas.2022490118

Canfield, D. E., & Berner, R. A. (1987). Dissolution and pyritization of magnetite in anoxie marine sediments. *Geochimica et Cosmochimica Acta*, *51*(3), 645–659. https://doi.org/10.1016/0016-7037(87)90076-7

Canfield, D. E., Raiswell, R., & Bottrell, S. (1992). The reactivity of sedimentary iron minerals toward sulfide. *American Journal of Science*, *292*(9), 659–683. https://doi.org/10.2475/ajs.292.9.659

Chang, L., Hong, H., Bai, F., Wang, S., Pei, Z., Paterson, G. A., et al. (2021). Detrital remanent magnetization of single-crystal silicates with magnetic inclusions: Constraints from deposition experiments. *Geophysical Journal International*, *224*(3), 2001–2015. https://doi.org/10.1093/gji/ggaa559

Chang, L., Roberts, A. P., Heslop, D., Hayashida, A., Li, J., Zhao, X., et al. (2016). Widespread occurrence of silicate-hosted magnetic mineral inclusions in marine sediments and their contribution to paleomagnetic recording. *Journal of Geophysical Research: Solid Earth*, *121*(12), 8415–8431. https://doi.org/10.1002/2016JB013109

Channell, J. E. T., Singer, B. S., & Jicha, B. R. (2020). Timing of Quaternary geomagnetic reversals and excursions in volcanic and sedimentary archives. *Quaternary Science Reviews*, *228*, 106114. https://doi.org/10.1016/j.quascirev.2019.106114

Channell, J. E. T., & Xuan, C. (2009). Self-reversal and apparent magnetic excursions in Arctic sediments. *Earth and Planetary Science Letters*, *284*(1–2), 124–131. https://doi.org/10.1016/j.epsl.2009.04.020

Chen, L., Heslop, D., Roberts, A. P., Chang, L., Zhao, X., McGregor, H. V., et al. (2017). Remanence acquisition efficiency in biogenic and detrital magnetite and recording of geomagnetic paleointensity. *Geochemistry, Geophysics, Geosystems*, *18*(4), 1435–1450. https://doi.org/10.1002/2016GC006753

Constable, C., Korte, M., & Panovska, S. (2016). Persistent high paleosecular variation activity in southern hemisphere for at least 10 000 years. *Earth and Planetary Science Letters*, *453*, 78–86. https://doi.org/10.1016/j.epsl.2016.08.015

Cullen, V. L., Smith, V. C., & Arz, H. W. (2014). The detailed tephrostratigraphy of a core from the south-east Black Sea spanning the last ~60 ka. *Journal of Quaternary Science*, *29*(7), 675–690. https://doi.org/10.1002/jqs.2739

Davies, C., & Constable, C. (2017). Geomagnetic spikes on the core-mantle boundary. *Nature Communications*, *8*(May), 1–11. https://doi.org/10.1038/ncomms15593

Dekkers, M. J., & Rochette, P. (1992). Magnetic properties of chemical remanent magnetization in synthetic and natural goethite: Prospects for a natural remanent magnetization/thermoremenant magnetization ratio paleomagnetic stability test? *Journal of Geophysical Research*, *97*(B12), 17291. https://doi.org/10.1029/92JB01026

Dillon, M., & Franke, C. (2009). Diagenetic alteration of natural Fe-Ti oxides identified by energy dispersive spectroscopy and low-temperature magnetic remanence and hysteresis measurements. *Physics of the Earth and Planetary Interiors*, *172*(3–4), 141–156. https://doi.org/10.1016/j.pepi.2008.08.003

Ebert, Y., Shaar, R., & Stein, M. (2021). Decadal geomagnetic secular variations from greigite bearing Dead Sea sediments. *Geochemistry, Geophysics, Geosystems*, *22*, 1–15. https://doi.org/10.1029/2021gc009665

Egger, M., Kraal, P., Jilbert, T., Sulu-Gambari, F., Sapart, C. J., Röckmann, T., & Slomp, C. P. (2016). Anaerobic oxidation of methane alters sediment records of sulfur, iron and phosphorus in the Black Sea. *Biogeosciences*, *13*(18), 5333–5355. https://doi.org/10.5194/bg-13-5333-2016

Feinberg, J. M., Scott, G. R., Renne, P. R., & Wenk, H. R. (2005). Exsolved magnetite inclusions in silicates: Features determining their remanence behavior. *Geology*, *33*(6), 513–516. https://doi.org/10.1130/G21290.1

Gehring, A. U. U., Mastrogiacomo, G., Fischer, H., Weidler, P. G. G., Müller, E., & Luster, J. (2008). Magnetic metastability in natural hemo-ilmenite solid solution (y≈0.83). *Journal of Magnetism and Magnetic Materials*, *320*(23), 3307–3312. https://doi.org/10.1016/j.jmmm.2008.06.038

Genevey, A., Gallet, Y., Jesset, S., Thébault, E., Bouillon, J., Lefèvre, A., & Le Goff, M. (2016). New archeointensity data from French Early Medieval pottery production (6th–10th century AD). Tracing 1500 years of geomagnetic field intensity variations in Western Europe. *Physics of the Earth and Planetary Interiors*, *257*, 205–219. https://doi.org/10.1016/j.pepi.2016.06.001

Gilder, S. A., He, K., Wack, M., & Ježek, J. (2019). Relative paleointensity estimates from magnetic anisotropy : Proof of concept. *Earth and Planetary Science Letters*, *519*, 83–91. https://doi.org/10.1016/j.epsl.2019.05.003

Gómez-Paccard, M., Chauvin, A., Lanos, P., Dufresne, P., Kovacheva, M., Hill, M. J., et al. (2012). Improving our knowledge of rapid geomagnetic field intensity changes observed in Europe between 200 and 1400 AD. *Earth and Planetary Science Letters*, *355*(356), 131–143. https://doi.org/10.1016/j.epsl.2012.08.037

He, K., Zhao, X., Pan, Y., Zhao, X., Qin, H., & Zhang, T. (2020). Benchmarking component analysis of remanent magnetization curves with a synthetic mixture series: Insight into the reliability of unmixing natural samples. *Journal of Geophysical Research: Solid Earth*, *125*, 1–16. https://doi.org/10.1029/2020jb020105

Heslop, D., & Roberts, A. P. (2020). Uncertainty propagation in hierarchical paleomagnetic reconstructions. *Journal of Geophysical Research: Solid Earth*, *125*(6), 1–12. https://doi.org/10.1029/2020JB019488

Höflmayer, F. (2012). The date of the minoan Santorini eruption: Quantifying the "offset. *Radiocarbon*, *54*(3–4), 435–448. https://doi.org/10.1017/S0033822200047196

Hong, H., Chang, L., Hayashida, A., Roberts, A. P., Heslop, D., Paterson, G. A., et al. (2019). Paleomagnetic recording efficiency of sedimentary magnetic mineral inclusions: Implications for relative paleointensity determinations. *Journal of Geophysical Research: Solid Earth*, *124*(7), 6267–6279. https://doi.org/10.1029/2018JB016859

Hounslow, M. W. (1996). Ferrimagnetic Cr and Mn spinels in sediments: Residual magnetic minerals after diagenetic dissolution. *Geophysical Research Letters*, *23*(20), 2823–2826. https://doi.org/10.1029/96GL01327

Hounslow, M. W., Maher, B. A., & Thistlewood, L. (1995). Magnetic mineralogy of sandstones from the Lunde Formation (late Triassic), northern North sea, UK: Origin of the palaeomagnetic signal. *Geological Society Special Publication*, *98*(98), 119–147. https://doi.org/10.1144/GSL.SP.1995.098.01.07

Hus, J. J. (1990). *The Magnetic Properties of Siderite Concretions and the CRM of Their Oxidation Products* (Vol. 63). https://doi.org/10.1016/0031-9201(90)90058-6

Jiang, X. D., Zhao, X. Y., Zhao, X., Jiang, Z. X., Chou, Y. M., Zhang, T. W., et al. (2021). Quantifying contributions of magnetic inclusions within silicates to marine sediments: A dissolution approach to isolating volcanic signals for improved paleoenvironmental reconstruction. *Journal of Geophysical Research: Solid Earth*, *126*(10), 1–18. https://doi.org/10.1029/2021jb022680

Jørgensen, B. B., Böttcher, M. E., Lüschen, H., Neretin, L. N., & Volkov, I. I. (2004). Anaerobic methane oxidation and a deep H2S sink generate isotopically heavy sulfides in Black Sea sediments. *Geochimica et Cosmochimica Acta*, *68*(9), 2095–2118. https://doi.org/10.1016/j.gca.2003.07.017

Just, J., Dekkers, M. J., Von Dobeneck, T., Van Hoesel, A., & Bickert, T. (2012). Signatures and significance of aeolian, fluvial, bacterial and diagenetic magnetic mineral fractions in late quaternary marine sediments off Gambia, NW Africa. *Geochemistry, Geophysics, Geosystems*, *13*(1). https://doi.org/10.1029/2012GC004146

Just, J., Sagnotti, L., Nowaczyk, N. R., Francke, A., & Wagner, B. (2019). Recordings of fast paleomagnetic reversals in a 1.2 Ma Greigite-rich sediment archive from Lake Ohrid, Balkans. *Journal of Geophysical Research: Solid Earth*, *124*(12), 12445–12464. https://doi.org/10.1029/2019JB018297

Katari, K., & Tauxe, L. (2000). Effects of pH and salinity on the intensity of magnetization in redeposited sediments. *Earth and Planetary Science Letters*, *181*(4), 489–496. https://doi.org/10.1016/S0012-821X(00)00226-0

Kirschvink, J. L. (1980). The least-squares line and plane and the analysis of palaeomagnetic data. *Geophysical Journal International*, *62*(3), 699–718. https://doi.org/10.1111/j.1365-246X.1980.tb02601.x

Korte, M., & Constable, C. G. (2018). Archeomagnetic intensity spikes: Global or regional geomagnetic field features? *Frontiers of Earth Science*, *6*(March), 1–15. https://doi.org/10.3389/feart.2018.00017

Kovacheva, M., Kostadinova-Avramova, M., Jordanova, N., Lanos, P., & Boyadzhiev, Y. (2014). Extended and revised archaeomagnetic database and secular variation curves from Bulgaria for the last eight millennia. *Physics of the Earth and Planetary Interiors*, *236*, 79–94. https://doi.org/10.1016/j.pepi.2014.07.002

Kwiecien, O., Arz, H. W., Lamy, F., Wulf, S., Bahr, A., Röhl, U., & Haug, G. H. (2008). Estimated reservoir ages of the black sea since the last glacial. *Radiocarbon*, *50*(1), 99–118. https://doi.org/10.1017/S0033822200043393

Lamy, F., Arz, H. W., Bond, G. C., Bahr, A., & Pätzold, J. (2006). Multicentennial-scale hydrological changes in the Black Sea and northern red Sea during the holocene and the Arctic/North Atlantic oscillation. *Paleoceanography*, *21*(1). https://doi.org/10.1029/2005pa001184

Larrasoaña, J. C., Roberts, A. P., Stoner, J. S., Richter, C., & Wehausen, R. (2003). A new proxy for bottom-water ventilation in the eastern Mediterranean based on diagenetically controlled magnetic properties of sapropel-bearing sediments. *Palaeogeography, Palaeoclimatology, Palaeoecology*, *190*, 221–242. https://doi.org/10.1016/S0031-0182(02)00607-7

Lawson, C. A., & Nord, G. L. (1984). Remanent magnetization of a "paramagnetic" composition in the ilmenite-hematite solid solution series. *Geophysical Research Letters*, *11*(3), 197–200. https://doi.org/10.1029/GL011i003p00197

Liu, J., Nowaczyk, N. R., Frank, U., & Arz, H. (2019). Geomagnetic paleosecular variation record spanning from 40 to 20 ka – Implications for the Mono Lake excursion from Black Sea sediments. *Earth and Planetary Science Letters*, *509*, 114–124. https://doi.org/10.1016/j.epsl.2018.12.029

Liu, J., Nowaczyk, N. R., Panovska, S., Korte, M., & Arz, H. W. (2020). The Norwegian-Greenland Sea, the Laschamps, and the mono lake excursions recorded in a Black Sea sedimentary sequence spanning from 68.9 to 14.5 ka. *Journal of Geophysical Research: Solid Earth*, *125*(8). https://doi.org/10.1029/2019JB019225

Liu, J., Shi, X., Liu, Q., Ge, S., Liu, Y., Yao, Z., et al. (2014). Magnetostratigraphy of a greigite-bearing core from the south Yellow sea: Implications for remagnetization and sedimentation. *Journal of Geophysical Research: Solid Earth*, *119*(10), 7425–7441. https://doi.org/10.1002/2014JB011206

Lund, S., Stoner, J. S., Channell, J. E. T., & Acton, G. (2006). A summary of Brunhes paleomagnetic field variability recorded in Ocean Drilling Program cores. *Physics of the Earth and Planetary Interiors*, *156*(3–4), 194–204. https://doi.org/10.1016/j.pepi.2005.10.009

Major, C. O., Goldstein, S. L., Ryan, W. B. F. F., Lericolais, G., Piotrowski, A. M., & Hajdas, I. (2006). The co-evolution of Black Sea level and composition through the last deglaciation and its paleoclimatic significance. *Quaternary Science Reviews*, *25*(17–18), 2031–2047. https://doi.org/10.1016/j.quascirev.2006.01.032

Molina-Cardín, A., Campuzano, S. A., Osete, M. L., Rivero-Montero, M., Pavón-Carrasco, F. J., Palencia-Ortas, A., et al. (2018). Updated Iberian archeomagnetic catalogue: New full vector paleosecular variation Curve for the Last 3 Millennia. *Geochemistry, Geophysics, Geosystems*, *19*, 3637–3656. https://doi.org/10.1029/2018GC007781

Neretin, L. N., Böttcher, M. E., Jørgensen, B. B., Volkov, I. I., Lüschen, H., & Hilgenfeldt, K. (2004). Pyritization processes and greigite formation in the advancing sulfidization front in the upper Pleistocene sediments of the Black Sea. *Geochimica et Cosmochimica Acta*, *68*(9), 2081–2093. https://doi.org/10.1016/S0016-7037(03)00450-2

Nowaczyk, N. R. (2011). Dissolution of titanomagnetite and sulphidization in sediments from Lake Kinneret, Israel. *Geophysical Journal International*, *187*(1), 34–44. https://doi.org/10.1111/j.1365-246X.2011.05120.x

Nowaczyk, N. R., Arz, H. W. W., Frank, U., Kind, J., & Plessen, B. (2012). Dynamics of the Laschamp geomagnetic excursion from Black Sea sediments. *Earth and Planetary Science Letters*, *351*(352), 54–69. https://doi.org/10.1016/j.epsl.2012.06.050

Nowaczyk, N. R., Frank, U., Kind, J., & Arz, H. W. (2013). A high-resolution paleointensity stack of the past 14 to 68 ka from black sea sediments. *Earth and Planetary Science Letters*, *384*, 1–16. https://doi.org/10.1016/j.epsl.2013.09.028

Nowaczyk, N. R., Jiabo, L., Frank, U., & Arz, H. W. (2018). A high-resolution paleosecular variation record from Black Sea sediments indicating fast directional changes associated with low field intensities during marine isotope stage (MIS) 4. *Earth and Planetary Science Letters*, *484*, 15–29. https://doi.org/10.1016/j.epsl.2017.12.009

Nowaczyk, N. R., Liu, J., & Arz, H. W. (2020). Records of the Laschamps geomagnetic polarity excursion from Black Sea sediments: Magnetite versus greigite, discrete sample versus U-channel data. *Geophysical Journal International*, *224*(2), 1079–1095. https://doi.org/10.1093/gji/ggaa506

Nowaczyk, N. R., Liu, J., & Arz, H. W. (2021a). Rock magnetic data from sediments from the Arkhangelsky ridge, SE Black Sea: I - cores from expedition M72/5, German RV Meteor, 2007. *GFZ Data Services*. https://doi.org/10.5880/GFZ.4.3.2021.002

Nowaczyk, N. R., Liu, J., & Arz, H. W. (2021b). Rock magnetic data from sediments from the Arkhangelsky ridge, SE Black Sea, II - Cores from expedition MSM33, German RV Maria S. Merian, 2013. *GFZ Data Services*. https://doi.org/10.5880/GFZ.4.3.2021.003

Osete, M. L., Molina-Cardín, A., Campuzano, S. A., Aguilella-Arzo, G., Barrachina-Ibañez, A., Falomir-Granell, F., et al. (2020). Two archaeomagnetic intensity maxima and rapid directional variation rates during the Early Iron Age observed at Iberian coordinates. Implications on the evolution of the Levantine Iron Age Anomaly. *Earth and Planetary Science Letters*, *533*, 116047. https://doi.org/10.1016/j.epsl.2019.116047

Panovska, S., Constable, C. G., & Korte, M. (2018). Extending global continuous geomagnetic field reconstructions on timescales beyond human civilization. *Geochemistry, Geophysics, Geosystems*, *19*, 1–16. https://doi.org/10.1029/2018GC007966

Panovska, S., Korte, M., & Constable, C. G. G. (2019). One hundred thousand years of geomagnetic field evolution. *Reviews of Geophysics*, *57*(4), 1289–1337. https://doi.org/10.1029/2019RG000656

Peckmann, J., Reimer, A., Luth, U., Luth, C., Hansen, B. T., Heinicke, C., et al. (2001). Methane-derived carbonates and authigenic pyrite from the northwestern Black Sea. *Marine Geology*, *177*(1–2), 129–150. https://doi.org/10.1016/S0025-3227(01)00128-1

Raiswell, R., & Canfield, D. E. (1998). Sources of iron for pyrite formation in marine sediments. *American Journal of Science*, *298*(3), 219–245. https://doi.org/10.2475/ajs.298.3.219

Riedinger, N., Brunner, B., Krastel, S., Arnold, G. L., Wehrmann, L. M., Formolo, M. J., et al. (2017). Sulfur cycling in an iron oxide-dominated, dynamic marine depositional system: The argentine continental margin. *Frontiers of Earth Science*, *5*(May). https://doi.org/10.3389/feart.2017.00033

Rivero-Montero, M., Gómez-Paccard, M., Kondopoulou, D., Tema, E., Pavón-carrasco, F. J., Aidona, E., et al. (2021). Geomagnetic field intensity changes in the central Mediterranean between 1500 BCE and 150 CE: Implications for the Levantine iron age anomaly evolution. *Earth and Planetary Science Letters*, *557*, 116732. https://doi.org/10.1016/j.epsl.2020.116732

Rivero-Montero, M., Gómez-Paccard, M., Pavón-Carrasco, F. J., Cau-Ontiveros, M. A., Fantuzzi, L., Martín-Hernández, F., et al. (2021). Refining geomagnetic field intensity changes in Europe between 200 CE and 1800 CE. New data from the Mediterranean region. *Physics of the Earth and Planetary Interiors*, *317*(February), 106749. https://doi.org/10.1016/j.pepi.2021.106749

Roberts, A. P. (2015). Magnetic mineral diagenesis. *Earth-Science Reviews*, *151*, 1–47. https://doi.org/10.1016/j.earscirev.2015.09.010

Roberts, A. P., & Winklhofer, M. (2004). Why are geomagnetic excursions not always recorded in sediments? Constraints from post-depositional remanent magnetization lock-in modelling. *Earth and Planetary Science Letters*, *227*(3–4), 345–359. https://doi.org/10.1016/j.epsl.2004.07.040

Robinson, P., Harrison, R. J., McEnroe, S. A., & Hargraves, R. B. (2002). Lamellar magnetism in the haematite-ilmenite series as an explanation for strong remanent magnetization. *Nature*, *418*(6897), 517–520. https://doi.org/10.1038/nature00942

Rowan, C. J., Roberts, A. P., & Broadbent, T. (2009). Reductive diagenesis, magnetite dissolution, greigite growth and paleomagnetic smoothing in marine sediments: A new view. *Earth and Planetary Science Letters*, *277*(1–2), 223–235. https://doi.org/10.1016/j.epsl.2008.10.016

Scheidt, S., Egli, R., Frederichs, T., Hambach, U., & Rolf, C. (2017). A mineral magnetic characterization of the Plio-Pleistocene fluvial infill of the Heidelberg Basin (Germany). *Geophysical Journal International*, *210*(2), 743–764. https://doi.org/10.1093/gji/ggx154

Selkin, P. A., Gee, J. S., Tauxe, L., Meurer, W. P., & Newell, A. J. (2000). The effect of remanence anisotropy on paleointensity estimates: A case study from the archean Stillwater Complex. *Earth and Planetary Science Letters*, *183*(3–4), 403–416. https://doi.org/10.1016/S0012-821X(00)00292-2

Shaar, R., Tauxe, L., Ron, H., Ebert, Y., Zuckerman, S., Finkelstein, I., & Agnon, A. (2016). Large geomagnetic field anomalies revealed in Bronze to iron age archeomagnetic data from Tel Megiddo and Tel Hazor, Israel. *Earth and Planetary Science Letters*, *442*, 173–185. https://doi.org/10.1016/j.epsl.2016.02.038

Shumilovskikh, L. S., Marret, F., Fleitmann, D., Arz, H. W., Nowaczyk, N. R., & Behling, H. (2013). Eemian and Holocene sea-surface conditions in the southern Black Sea: Organic-walled dinoflagellate cyst record from core 22-GC3. *Marine Micropaleontology*, *101*, 146–160. https://doi.org/10.1016/j.marmicro.2013.02.001

Snowball, I. F. (1997). Gyroremanent magnetization and the magnetic properties of greigite-bearing clays in southern Sweden. *Geophysical Journal International*, *129*(3), 624–636. https://doi.org/10.1111/j.1365-246X.1997.tb04498.x

Snowball, I. F., & Thompson, R. (1990). A stable chemical remanence in Holocene sediments. *Journal of Geophysical Research*, *95*(B4), 4471. https://doi.org/10.1029/JB095iB04p04471

Soulet, G., Ménot, G., Garreta, V., Rostek, F., Zaragosi, S., Lericolais, G., & Bard, E. (2011). Black Sea "lake" reservoir age evolution since the last glacial - Hydrologic and climatic implications. *Earth and Planetary Science Letters*, *308*(1–2), 245–258. https://doi.org/10.1016/j.epsl.2011.06.002

Stoner, J., Laj, C., Channell, J. E., & Kissel, C. (2002). South Atlantic and North Atlantic geomagnetic paleointensity stacks (0–80ka): Implications for inter-hemispheric correlation. *Quaternary Science Reviews*, *21*(10), 1141–1151. https://doi.org/10.1016/S0277-3791(01)00136-6

Strechie, C., André, F., Jelinowska, A., Tucholka, P., Guichard, F., Lericolais, G., & Panin, N. (2002). Magnetic minerals as indicators of major environmental change in holocene black sea sediments: Preliminary results. *Physics and Chemistry of the Earth, Parts A/B/C*, *27*(25–31), 1363–1370. https://doi.org/10.1016/S1474-7065(02)00119-5

Tarduno, J. A., Cottrell, R. D., & Smirnov, A. V. (2006). The paleomagnetism of single silicate crystals: Recording geomagnetic field strength during mixed polarity intervals, superchrons, and inner core growth. *Reviews of Geophysics*, *44*(1), 1–31. https://doi.org/10.1029/2005RG000189

Tarduno, J. A., Watkeys, M. K., Huffman, T. N., Cottrell, R. D., Blackman, E. G., Wendt, A., et al. (2015). Antiquity of the South Atlantic Anomaly and evidence for top-down control on the geodynamo. *Nature Communications*, *6*. https://doi.org/10.1038/ncomms8865

Tauxe, L. (1993). Sedimentary records of relative paleointensity of the geomagnetic field: Theory and practice. *Reviews of Geophysics*, *31*(3), 319. https://doi.org/10.1029/93RG01771

Tauxe, L., Steindorf, J. L., & Harris, A. (2006). Depositional remanent magnetization: Toward an improved theoretical and experimental foundation. *Earth and Planetary Science Letters*, *244*(3–4), 515–529. https://doi.org/10.1016/j.epsl.2006.02.003

Usui, Y., Shibuya, T., Sawaki, Y., & Komiya, T. (2015). Rock magnetism of tiny exsolved magnetite in plagioclase from a Paleoarchean granitoid in the Pilbara craton. *Geochemistry, Geophysics, Geosystems*, *16*(1), 112–125. https://doi.org/10.1002/2014GC005508

Valet, J.-P., & Fournier, A. (2016). Deciphering records of geomagnetic reversals. *Reviews of Geophysics*, *54*(2), 410–446. https://doi.org/10.1002/2015RG000506

Wegwerth, A., Eckert, S., Dellwig, O., Schnetger, B., Severmann, S., Weyer, S., et al. (2018). Redox evolution during Eemian and holocene sapropel formation in the Black Sea. *Palaeogeography, Palaeoclimatology, Palaeoecology*, *489*(July), 249–260. https://doi.org/10.1016/j.palaeo.2017.10.014

Wiers, S., Snowball, I. F., O'Regan, M., & Almqvist, B. (2019). Late pleistocene chronology of sediments from the Yermak Plateau and uncertainty in dating based on geomagnetic excursions. *Geochemistry, Geophysics, Geosystems*, *20*(7), 1–22. https://doi.org/10.1029/2018gc007920

Wilkin, R. T., Arthur, M., & Dean, W. (1997). History of water-column anoxia in the Black Sea indicated by pyrite framboid size distributions. *Earth and Planetary Science Letters*, *148*(3–4), 517–525. https://doi.org/10.1016/S0012-821X(97)00053-8

Wilkin, R. T., Barnes, H. L., & Brantley, S. L. (1996). The size distribution of framboidal pyrite in modern sediments: An indicator of redox conditions. *Geochimica et Cosmochimica Acta*, *60*(20), 3897–3912. https://doi.org/10.1016/0016-7037(96)00209-8

Wilson, G. S., & Roberts, A. P. (1999). Diagenesis of magnetic mineral assemblages in multiply redeposited siliciclastic marine sediments, Wanganui basin, New Zealand. *Geological Society, London, Special Publications*, *151*, 95–108. https://doi.org/10.1144/GSL.SP.1999.151.01.10

Wirth, R. (2004). Focused Ion Beam (FIB): A novel technology for advanced application of micro- and nanoanalysis in geosciences and applied mineralogy. *European Journal of Mineralogy*, *16*(6), 863–876. https://doi.org/10.1127/0935-1221/2004/0016-0863

Wirth, R. (2009). Focused Ion Beam (FIB) combined with SEM and TEM: Advanced analytical tools for studies of chemical composition, microstructure and crystal structure in geomaterials on a nanometre scale. *Chemical Geology*, *261*(3–4), 217–229. https://doi.org/10.1016/j.chemgeo.2008.05.019

Yu, Y., & Tikoff, B. (2020). Magnetic Cr-rich spinel in serpentinized ultramafic complexes. *Journal of Geophysical Research: Solid Earth*, *125*(11). https://doi.org/10.1029/2020jb020443

Zhao, X., Heslop, D., & Roberts, A. P. (2015). A protocol for variable-resolution first-order reversal curve measurements. *Geochemistry, Geophysics, Geosystems*, *16*, 1364–1377. https://doi.org/10.1002/2014GC005680

Zhao, X., Roberts, A. P., Heslop, D., Paterson, G. A., Li, Y., & Li, J. (2017). Magnetic domain state diagnosis using hysteresis reversal curves. *Journal of Geophysical Research: Solid Earth*, *122*(7), 4767–4789. https://doi.org/10.1002/2016JB013683